SIMULATION OF THE EFFECT OF MICROSTRUCTURE ON ELECTROMIGRATION INDUCED FAILURE OF INTERCONNECTS

by

WALID R. FAYAD

Ingenieur de L'Ecole Polytechnique, France, 1995
Ingenieur de l'Ecole Centrale de Paris, France, 1995

Submitted to the Department of Civil and Environmental Engineering
in Partial Fulfillment of the Requirements for the Degree of

MASTER OF SCIENCE IN CIVIL AND ENVIRONMENTAL ENGINEERING

at the

MASSACHUSETTS INSTITUTE OF TECHNOLOGY

June 1997

© 1997 Massachusetts Institute of Technology
All Rights Reserved

Signature of Author____________________________________
Department of Civil and Environmental Engineering
February 15, 1997

Certified by____________________________________
Carl V. Thompson
Professor of Electronic Materials
Thesis Supervisor

Certified by____________________________________
Jerome J. Connor
Professor of Civil and Environmental Engineering
Thesis Reader

Accepted by________
Joseph M. Sussman
Chairman, Departmental Committee on Graduate Studies

MASSACHUSETTS INSTITUTE OF TECHNOLOGY

JUN 24 1997

Eng.

SIMULATION OF THE EFFECT OF MICROSTRUCTURE ON ELECTROMIGRATION INDUCED FAILURE OF INTERCONNECTS

by

WALID R. FAYAD

Submitted to the Department of Civil and Environmental Engineering on February 15, 1997 in partial fulfillment of the requirements for the degree of Master of Science in Civil and Environmental Engineering

ABSTRACT

The geometry and microstructure of interconnects have a dramatic effect on their times to failure due to electromigration. An existing grain growth program was substantially modified to simulate the patterning of interconnect features of general shapes from polygranular thin film structures with lognormal grain size distributions. The program was used in the case of rectangular patterns to investigate the microstructure of straight line interconnects. In this case, depending on the line-width to median-grain-diameter ratio (W/D_{50}), the grain structure of a line may be composed of either all bamboo grains, polygranular clusters, or more likely, some mixture of the two. For relatively low values of W/D_{50}, ($W/D_{50}<0.5$) the maximum cluster length is small and the effect of the line length on cluster length distribution is negligible. For larger values of W/D_{50}, end effects are negligible as long as the line is longer than the maximum cluster length for an infinite line with the same width.

A statistical description of the microstructure of straight line interconnects is derived from the grain growth program. Polygranular cluster and bamboo-region length distributions are found to obey a Weibull distribution for a wide range of W/D_{50}, ($0.1<W/D_{50}<1$), but in the case of clusters in relatively wide lines ($W/D_{50}>0.5$), the lognormal distribution provides a better approximation.

These results were used in conjunction with the information provided by the grain growth program on the descriptive distribution statistical parameters to develop a program to generate lines with realistic microstructures without the use of the simulator. This program was linked to an electromigration simulation program to evaluate the statistics of the times to electromigration-induced interconnect failures, as a function of line-width, grain size, line-length, current density and temperature. A web-based version of the new simulation tool was created and is available for use by enginneers in the integrated circuit industry.

Thesis Supervisor: Carl V. Thompson, Professor of Electronic Materials.

Acknowledgments

Thank you to Professor Carl Thompson, my thesis advisor, with whom I am truly lucky to be working. Not only has he always been guiding and encouraging, but also, he has continuously provided the environment for very enjoyable research.

Thank you to Professor Jerome Connor, the thesis reader, for his consistently enriching advice.

Thank you to Professor Harold Frost for our very enlightening discussions and his insightful comments.

To all the other people involved in this work, I say thank you. Thank you to Yonald, Vab and Matt who actively participated in the completion of this work. Thank you to Doctor Brett Knowlton for his help and cooperation. Thank you to Steve especially, for he is always ready to answer all my questions. And thank you to Morgan for helping out in all sorts of situations.

To all my friends, without whom life has no meaning, I say thank you. Especially, thanks to Shanti, Saad, Kamal, Ibrahim, Ziad and Richard for their constant support and help.

Last but not least, I would like to say thank you to my brother Bassam, who has always been there for me.

This work was supported by the Defense Advanced Research Projects Agency (D.A.R.P.A).

Table of Contents

Acknowledgments 3
List of Figures 5

1. Introduction 8
1.1 Motivation/Ultimate Goal........ 8
1.2 Grain Structure of a Polycrystalline Film........ 10
1.3 Electromigration-Induced Failure of Interconnects........ 10

2. Electromigration and Microstructure 16
2.1 Experimental Observations........ 16
2.2 Microstructure of Interconnect Lines and its Impact on Reliability........ 19
2.3 Analytic Model for the Microstructure of As-Patterned Lines........ 24
2.4 Analytic Model for As-Patterned Near-Bamboo Lines Reliability........ 27
2.5 Evaluation of the Previous Models and their Limitations 33

3. Simulation Package and its Modification 35
3.1 The Simulation Package........ 35
3.2 Generation of Interconnects with Various Geometries........ 39

4. Structure Statistics 44
4.1 End Effects on Microstructure Statistics of Straight Lines........ 44
4.2 Bamboo Length Distribution / Cluster Length Distribution........ 46

5. Implementation in the Electromigration Simulation Tool 54
5.1 The Electromigration Simulation Program........ 54
5.2 Reliability of Realistic Lines Generated with the Grain Growth Program..... 55
5.3 Using the Statistical Model to Predict Reliability of Interconnects........ 60

6. Immediate Tasks and Future Perspectives 70
6.1 Exploring As-Patterned General Features........ 70
6.2 Post-Patterning Annealing in General Shapes........ 73

Appendices 73
A. Modeling Electromigration-Induced Stress Evolution in Confined Metal Lines 77
B. Lognormal and Weibull Distributions 82
B.1 Lognormal Plot of a Cumulative Distribution Function........ 82
B.2 Weibull Plot of a Cumulative Distribution Function........ 83

References 85

List of Figures

Figure 1.1 Planar view of a 1μm thick Al-alloy polycrystalline thin film..................11

Figure 1.2 3-D picture of a thin film showing the columnar grain structure of metallizations..12

Figure 2.1 Median times to failure and deviation in the time to failure vs. line width/grain size ratio for Al-2%Cu-0.3%Cr lines..17

Figure 2.2 Median time to failure vs. current density for lines with different widths..18

Figure 2.3 (a) The grain structure of a continuous film, (b) a wide line, (c) a near-bamboo line mostly composed of bamboo grains. The wide line has a continuous grain boundary along the line length, and the bamboo line is composed of a series of single grains. The near-bamboo line has both polygranular clusters and bamboo grains............20

Figure 2.4 The predicted and measured average cluster lengths as a function w/D_{50}. Predicted average lengths from the model match the measured values well.....................26

Figure 2.5 The transition current density, j^*, dependence on w/D_{50}. Different lines represent different total line lengths, L_{tot}/D_{50}..28

Figure 2.6 The expected dependence of the median time to failure, t_{50}, on the current density j for the polygranular failure mechanism. Projection to lower densities requires experimental results for transgranular failure mechanisms..30

Figure 2.7 Predicted dependence of t_{50} on w/D_{50}..32

Figure 3.1 The Johnson-Mehl structure generated by the programs *nucleate* and *impinge*. The dots represent grain boundary sites...37

Figure 3.2 Etching lines using the *etch* program. These patterning lines will convert the film into a single, thin film band..37

Figure 3.3 (a) Patterning an L structure using the program *pattern*, (b) patterning a T structure with the same program..40

Figure 3.4 Schematic illustration of the patterning algorithm used by the program *pattern*. The routine repeatedly takes the next edge triple points couple, establishes the

links with the previous ones, as well as their surrounding neighbors. It also creates a new external grain and updates its links..42

Figure 4.1 End Effects on Microstructure statistics. Lognormal plot of cluster length distribution in 2 cases, (1) 1 semi-infinite line (L_{tot}/D_{50}=1550, W/D_{50}=0.41) etched with *etch*, and (2) a collection of 45 lines with the same width, and with finite length (L/D_{50}=34.75, this gives the same total length) etched with *pattern*. In this case where the length of the finite lines is relatively large compared to the line width (L/W=85), the difference observed is negligible..45

Figure 4.2 Lognormal Plot of Bamboo Length Distribution. The film structure is characterized by D_{50}=2.59, σ_d=0.28. The deviation of the residual observed is about 0.2..48

Figure 4.3 Weibull Plot of Bamboo Length Distribution. The residual standard deviation is here smaller by an order of magnitude than the case of a lognormal fit........49

Figure 4.4 W/D_{50} dependence of the Weibull parameters in the case of the Bamboo Length Distribution. As expected, α, which is proportional to the average segment length, decreases with increasing W/D_{50} while β has an almost constant value of 1.2................50

Figure 4.5 Comparison of the error in fitting a lognormal distribution vs a Weibull distribution in the case of clusters. While the Weibull distribution seems to describe well the distribution for small values of W/D_{50} (less than 0.5), the lognormal distribution fits better for wider lines (W/D_{50} more than 0.5)..52

Figure 4.6 Comparison of the error in fitting a lognormal distribution vs a Weibull distribution in the case of bamboo segments. The Weibull distribution fits better the for a wide range of values of W/D_{50} ($0.1 < W/D_{50} < 1.0$)..53

Figure 5.1 The stress as a function of position for a line containing a single 20 μm long polygranular cluster..56

Figure 5.2 The stress as a function of position for a line containing two 20 μm long polygranular clusters separated by 20 μm. The stress profiles from each cluster begin to interact at intermediate times, leading to larger stresses than either cluster could support independently..57

Figure 5.3 The maximum stress as a function of time for pure Al lines with two 10 μm long polygranular clusters with a variety of spacings at a typical test current density. Curves for isolated clusters are also shown as a reference...58

Figure 5.4 The maximum stress as a function of position for 10 as-patterned lines with zero stress boundary conditions. All of these lines have identical process histories.

The variation in microstructure from line to line accounts for the variation in stress evolution behavior [30]....61

Figure 5.5 Lognormal plot of failure time distributions for the lines considered in figure 5.4 for small, intermediate and large values of σ_{cr}. Polygranular failures are denoted by stars, and transgranular failures are denoted by circles. At intermediate values of σ_{cr}, two failure mechanisms are active, resulting in a bimodal distribution [30]....62

Figure 5.6 The Web interface for the electromigration simulation package. Interconnect lines are generated and electromigration simulations are performed according to the conditions entered by the user. A lognormal plot of the failure times is then displayed to the user....64

Figure 5.7 Lognormal plot of failure time distributions for 10 lines generated with a Weibull distribution of cluster lengths....65

Figure 5.8 Lognormal plot of failure time distributions for 10 lines generated with the grain growth simulator under the same conditions given in figure 5.5....66

Figure 5.9 Lognormal plot of failure time distributions for 10 lines generated with a Weibull distribution of cluster lengths. This population is different than the one in figure 5.7 but with the same characteristics....67

Figure 5.10 Lognormal plot of failure time distributions for a population of fifty lines generated with a Weibull distribution of cluster length....69

Figure 6.1 4 geometrical parameters for an L structure vs only 2 for a simple rectangular line (the width W and length L)....72

Figure A.1 Schematic of a confined interconnect line with a columnar grain structure. Also shown are the principal stresses, σ_1 along the line direction, σ_2 in the width (w) direction, and σ_3 in thickness (h) direction....78

Chapter 1

Introduction

1.1 Motivation / Ultimate Goal

Interconnects are the thin metal lines connecting the millions of electronic devices composing a single Integrated Circuit. These lines have various geometries and are obtained by depositing a thin metal film over a dielectric layer and then patterning it. Aluminum and Aluminum alloys are the most widely used metallization materials because of their ease of deposition, high electric conductivity, and good patternability, as well as their good adherence to the silicon substrate. However, when Aluminum interconnects are subjected to high current densities, they may fail due to a current-induced diffusive phenomenon called electromigration.

Electromigration-induced failure is the primary failure mechanism of modern integrated circuits. A major concern of the designers of high performance integrated circuits is therefore interconnect reliability. Design limits imposed due to metal reliability concerns are often very conservative. Worst case assumptions are often made because of the current absence of a sound basis for more accurate assessments. For example, a common assumption is to consider all lines in an IC to be at the maximum allowed current density, even though most are not. Also dc current assumptions are made although most lines are subjected to less damaging pulsed dc or bi-directional currents.

Most importantly, design practice is still generally based on worst case feature sizes assumptions. The cumulation of these worst case assumptions leads to designs with excessive reliability, and, therefore reduced performance.

It is now possible to use the newly available feature sizes extraction tools along with line-width and line-length dependent design rules to predict the reliability of individual circuit elements, leading to a significantly less conservative estimation of the overall reliability. However, these feature-size dependent design rules depend on details, such as the ways in which the lines end (e.g. at W-filled studs, pads...). These reliability rules are also strongly dependent on the internal grain structure of the metal, which in turn depends on the deposition process as well as the post-patterning thermal history. The process-sensitive feature size dependence of reliability is now known in some detail, and can, with further development and new tools, be used to more accurately assess circuit reliability.

We are developing a powerful design tool which can be used with improved IC feature extraction tools to calculate and apply process-sensitive reliability rules to reliability assessments of full or partial IC designs. The generation of the required array of rules requires a detailed knowledge of the grain structure and stress of the different interconnect elements. These evolve in ways which are already known for some features, such as straight flat lines. Simulations and analytic models describing the grain structure of straight flat lines exist, along with analytic models for relating the grain structure of straight long lines to their reliability. We are developing similar simulations and models for interconnect elements with other characteristics. Once these grain structure models

exist, along with stress evolution models, they can be used in process-sensitive reliability assessments.

1.2 Grain Structure of a Polycristalline Film

Figure 1.1 shows a planar view of a 1μm thick Al-alloy polycristalline thin film deposited on a silicon substrate. In such a structure, grains meet at geometrically well defined grain boundaries. Usually, the metallizations have a columnar grain structure, so that all grain boundaries are perpendicular to the plane of the substrate as depicted in figure 1.2. Atomic diffusion is faster by several orders of magnitude along these grain boundaries than through the grain lattices or along the metal interface with the substrate or the surrounding glass. This fact has a great impact on interconnect reliability as we will see in the second chapter of this report.

1.3 Electromigration-Induced Failure of Interconnects

High current densities in interconnects cause them to fail due to electromigration. Electromigration induced failure is one of the primary failure mechanisms of integrated circuits. The continuous miniaturization in the IC designs leads to interconnects with smaller cross-sections and therefore subjected to higher current densities, causing

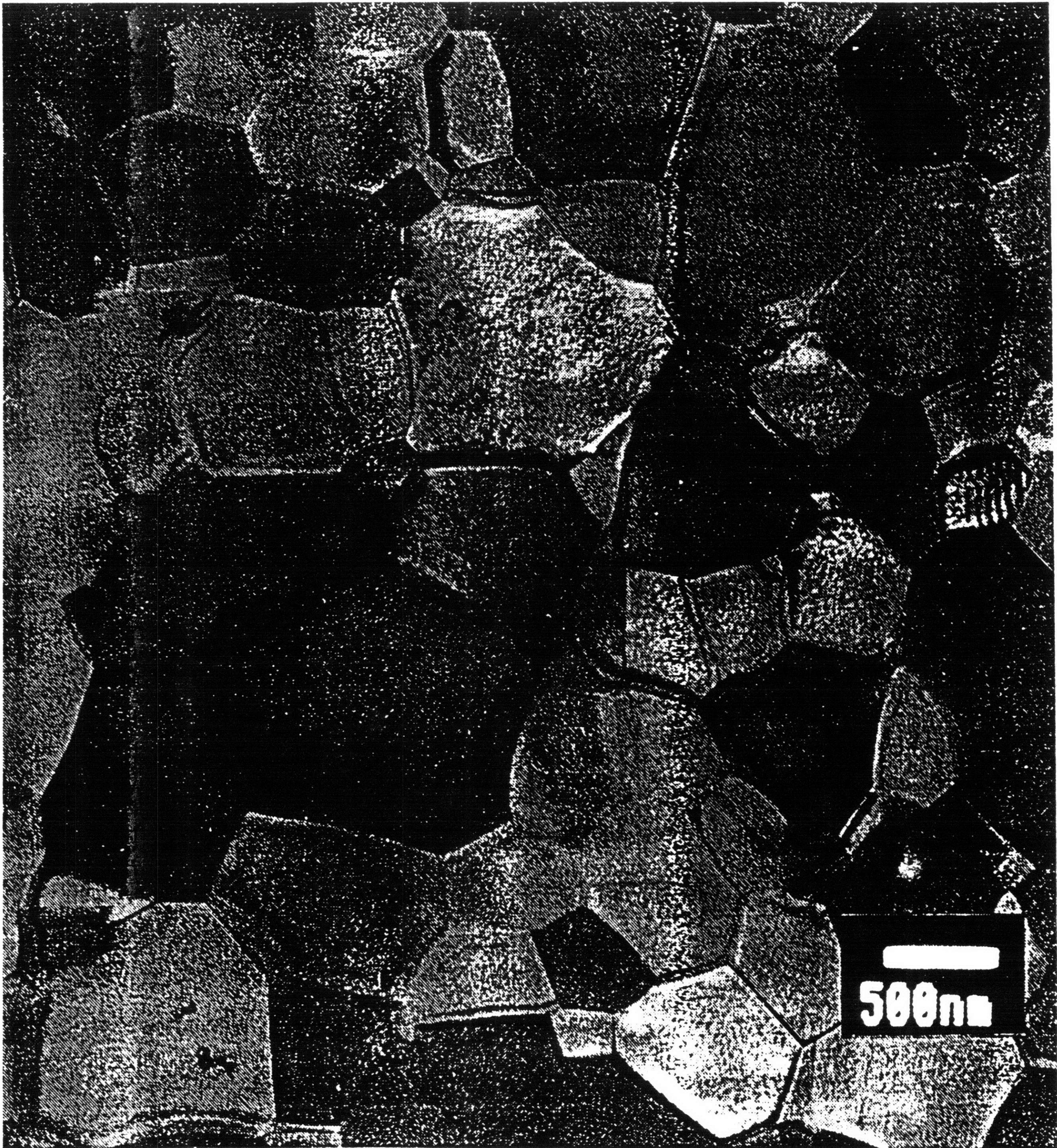

Figure 1.1 Planar view of a 1μm thick Al-alloy polycristalline thin film.

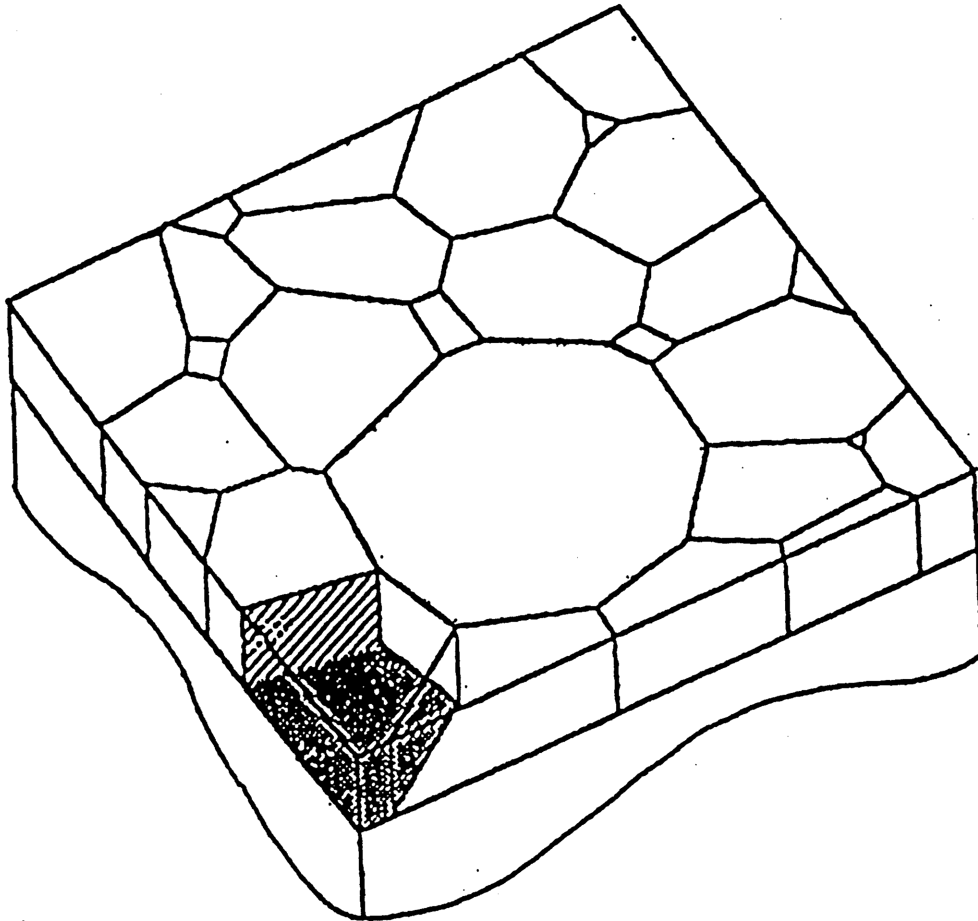

Figure 1.2 3-D picture of a thin film showing the columnar grain structure of metallizations.

electromigration to occur at an accelerated rate and increasing the risk of electromigration failure.

Electromigration refers to current-induced atomic diffusion due to a momentum transfer from the electrons to the atoms in the presence of an electric field. Momentum transfer causes the atoms to move in the direction of the electron flow. The flux of atoms due to the electron wind force can be expressed as the product of the mobility and the net driving force [1] by:

$$J = (\frac{DC}{kT})Z^{*}qE = (\frac{DC}{kT})Z^{*}q\rho j, \quad (1.1)$$

where D is the diffusivity, C is the concentration of the migrating atoms, k is Boltzmann's constant, Z^{*} is the effective charge of the atoms, q is the fundamental charge, E is the electric field, taken to be the product of the resistivity ρ by the current density j.

Electromigration-induced failure of interconnects occurs at sites of flux divergence. If the incoming flux of atoms is less than the outgoing flux, atoms are depleted from that site, forming a void. If the void spans the width of the line, open circuit failure usually results. On the other hand, if the incoming flux of atoms is greater than the outgoing one, the atoms accumulate, generating a hillock. The hillock can cause a fracture in the surrounding passivation layer, leading to Al extrusion and an electrical short circuit to a neighboring conductor. Microstructural features such as grain boundary triple junctions [2] and local variation in grain sizes [3], or local temperature changes [4], are the main causes of flux divergences in Al polycristalline lines.

Failure of interconnects strongly depends, as we have seen, on the microstructural characteristics of the lines. Therefore, interconnect lifetime prediction, or interconnect reliability, constitutes a statistical problem. Solving this problem is required for the design of integrated circuits. It can be done experimentally, or analytically based on simulations. The most common experimental procedure in evaluating electromigration-limited reliability is lifetime measurements under accelerated conditions (high temperature, e.g. 200-250°C, and high current density, e.g. 10^6 A/cm^2) [5]. A population of identical lines are tested under the same conditions in order to capture the lifetime statistics. The commonly agreed on results are that failure time statistics of interconnects obey a lognormal distribution characterized by a median time to failure (MTTF) t_{50} and a deviation in time to failure (DTTF) σ_f. The major problem in interconnect reliability prediction is how to scale the experimentally observed values of t_{50} and σ_f from test conditions to service conditions.

The conventional scaling methodology, still being used today in electromigration reliability assessments, is based on the following empirical relationship proposed by Black, and relating t_{50} to the temperature and current density:

$$t_{50} = Aj^{-n} \exp(\frac{E_a}{kT}), \qquad (1.2)$$

where A is a constant related to the geometry and microstructure of the lines, j is the current density, n is the current density exponent generally accepted to be equal to 2, E_a is the apparent activation energy of failure, the value of which is determined

experimentally and depends on the dominant diffusion mechanism (0.4-0.8 eV for Al-alloy interconnects), and T is the temperature.

This conventional methodology for electromigration induced failure characterization poses many problems. Although Black's equation predicts a current density dependence for the median time to failure, the current density dependence of the deviation in failure time is not predicted, and more importantly the relationship between the lifetime components, t_{50} and σ_f, and the lines geometrical characteristics (length and width for flat straight lines) is not determined. Also, the lines microstructure effect as well as the process dependence is not captured.

We propose to use experimentally sustained simulations, in order to develop analytic models for the dramatic effect of microstructure characteristics and feature sizes, as well as the effect of processing on interconnect reliability. As mentioned before, some of this work has been already accomplished for flat straight lines [6, 7] and will be presented in the next paragraph. The work in progress concerning the microstructural characteristics of more general interconnect geometries will be discussed in a following paragraph, and finally future work concerning the process dependence of reliability and the post-patterning annealing of interconnects will be presented.

Chapter 2

Electromigration and Microstructure

2.1 Experimental Observations

Cho and Thompson have demonstrated experimentally the dependence of failure times on the microstructure characteristics of the film the lines are etched from as well as on the lines geometrical characteristics [8]. Figure (2.1) shows the dependence of the MTTF t_{50} and the DTTF σ_f on the ratio of the line width and the median grain size. The use of narrower lines, or equivalently, of lines with larger grains, can enhance the median time to failure by a factor of 2. Similar results have shown that shorter lines have better reliability than longer ones. While a decrease in line width or length leads to an increase in t_{50}, it also leads to an increase in σ_f so that the effect on reliability of a population of interconnects is not immediately obvious.

The current density dependence of the median time to failure seems also to depend on the microstructure of the lines [9]. Atakov et al have shown that the j^{-2} dependence of the MTTF is only true for wide lines (meaning a large width compared to the grain size) at high currents, suggesting the existence of multiple failure modes for intermediate widths (widths comparable to the grain size) and at low currents instead of the conventional assumption of a monomodal failure distribution (figure 2.2). The microstructural explanation of the multiple failure mechanisms is going to be discussed in

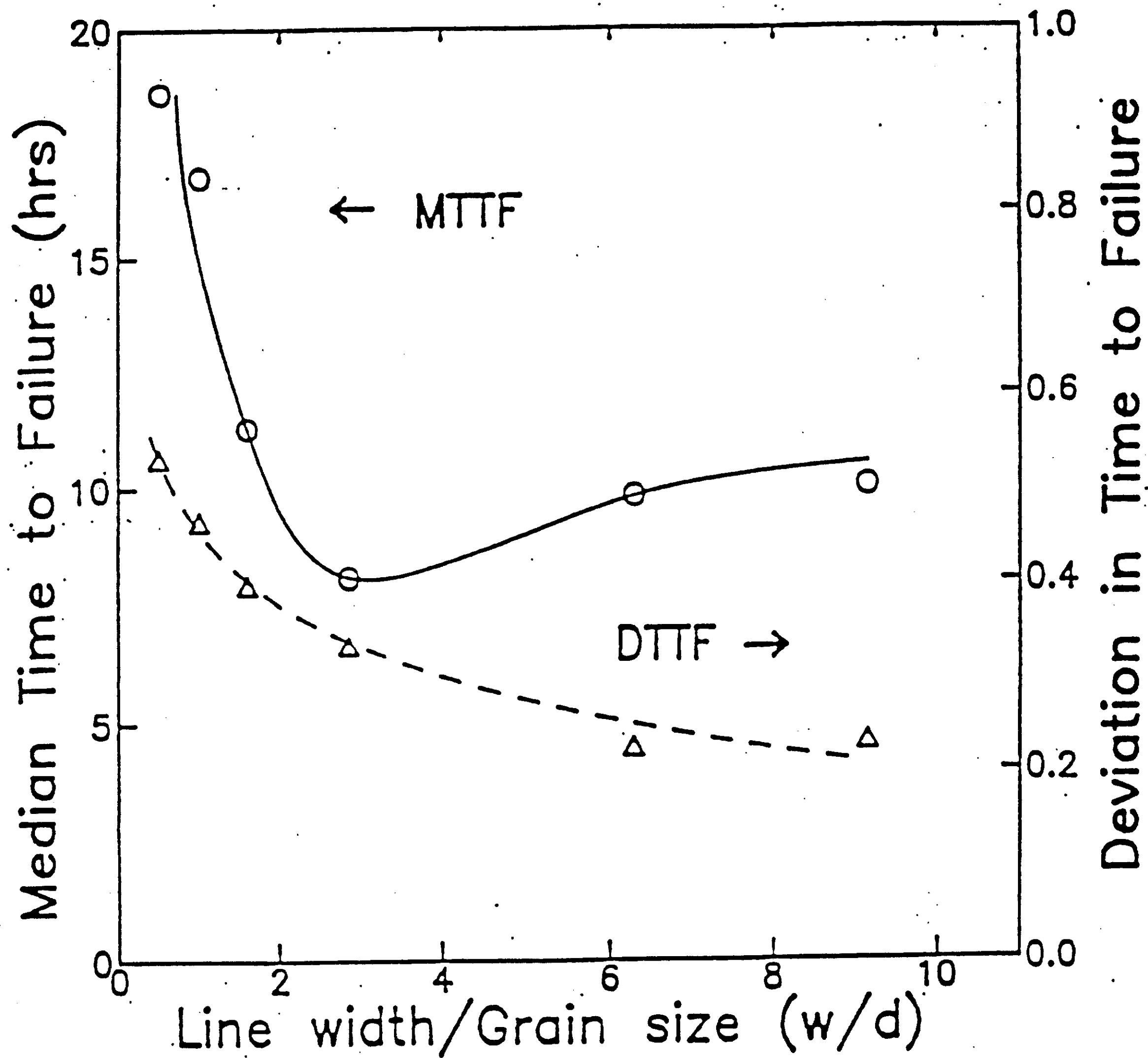

Figure 2.1 Median times to failure and deviation in the time to failure vs. line width/grain size ratio for Al-2%Cu-0.3%Cr lines.

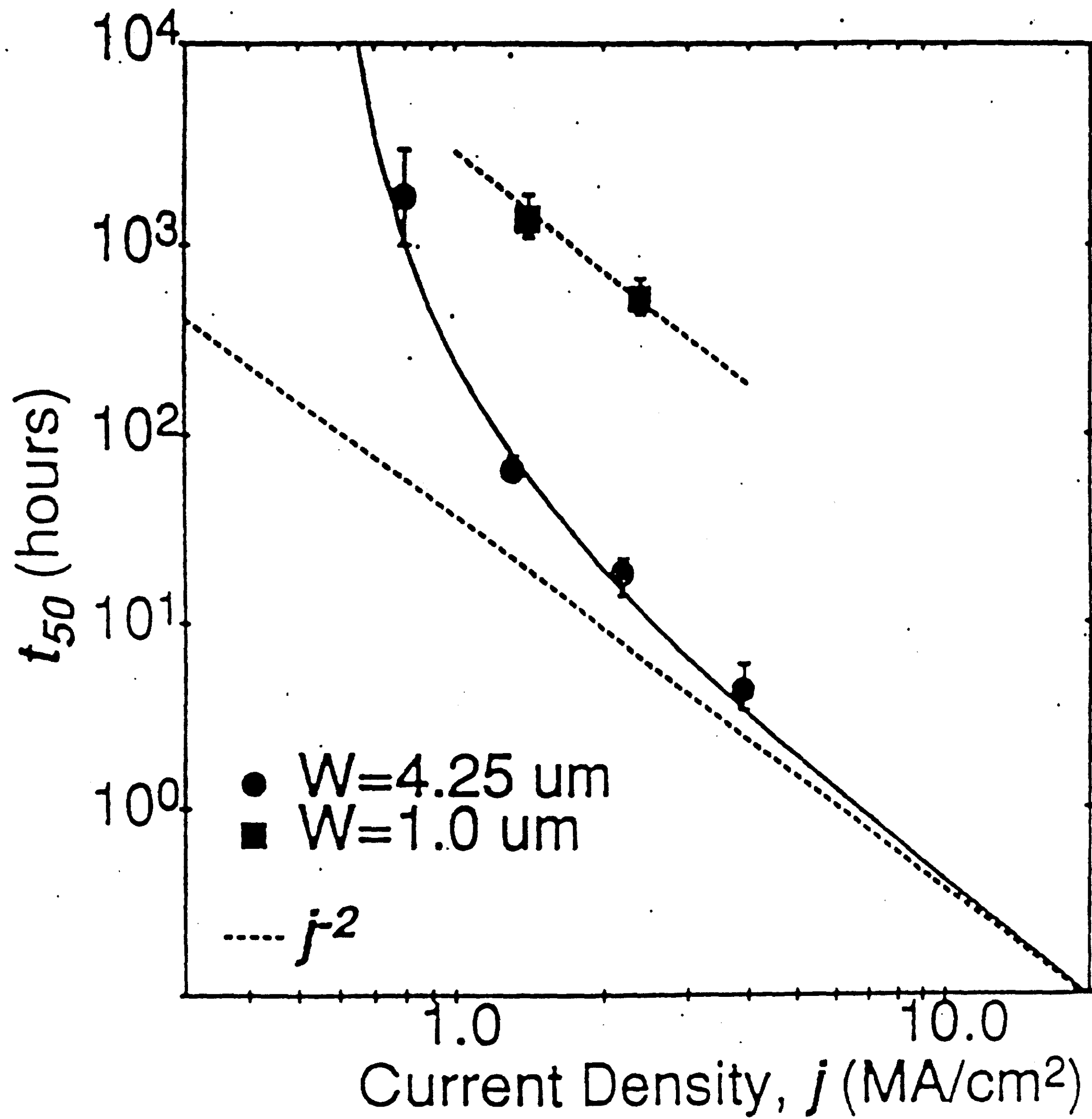

Figure 2.2 Median time to failure vs. current density for lines with different widths.

the following section along with a microstructure-sensitive analytic model for the reliability of flat straight lines.

2.2 Microstructure of Interconnect Lines and its Impact on Reliability

It has been well established that the sputter-deposition of Al and Al-alloys on an S_iO_2 layer usually leads to polycristalline thin films with lognormally distributed grain sizes [10, 11]. The in-plane-size or diameter is taken to be a measure of the average grain dimension. The grain size distribution is therefore characterized by two parameters, the median grain size D_{50}, and a variation in grain size σ_d, which is the standard deviation of ln(D). We have developed a simulation tool capable of generating grain structures that match the statistical characteristics that Al and Al-alloy films are known to have (figure 2.3 a). We also use an etching routine with this program to generate straight interconnect lines with different widths and lengths. Understanding the line grain structure is necessary for a correct assessment of the effect of microstructure on the electromigration response of the line.

When the width of the line is significantly greater than the median grain size of the film the line is etched from, the line displays a continuous network of grain boundaries (figure 2.3 b). As the width of the line decreases and approaches the median grain size, more grains span the width of the line, leading to a near-bamboo structure. In such a structure, we distinguish the *bamboo segments*, formed of one or many

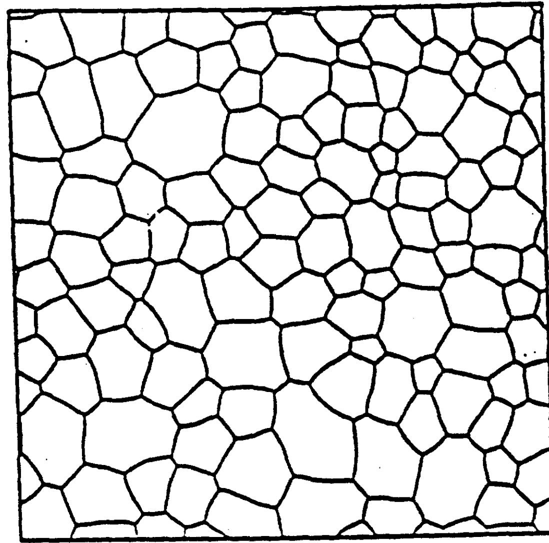
(a)

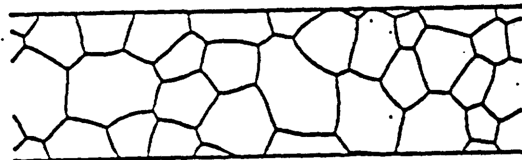
(b)

(c)

(d)

Figure 2.3 (a) The grain structure of a continuous film, (b) a wide line, (c) a near-bamboo line mostly composed of bamboo grains. The wide line has a continuous grain boundary along the line length, and the bamboo line is composed of a series of single grains. The near-bamboo line has both polygranular clusters and bamboo grains.

consecutive grains spanning the width of the line, from the *polygranular clusters* which are segments with a continuous grain boundary pathway along the length of the line (figure 2.3 c). When the width of the line becomes much smaller than the median grain size, we obtain a fully-bamboo structure with few if any polygranular clusters in the line (figure 2.3 d).

Electromigration, or current induced diffusion, in these polycristalline lines is dominated by two different mechanisms. In bamboo segments, where no grain boundary pathway lies along the line length, atomic diffusion occurs along the aluminum-oxide interface or through the lattice. However, in the polygranular clusters, diffusion occurs primarily along the grain boundaries because of the much higher atomic diffusivity of those compared to the lattice diffusivity or even to the aluminum oxide interface diffusivity.

Electromigration failure of interconnect lines, which usually have a near-bamboo grain structure, is coupled to the line's microstucture through the difference in diffusivity in polygranular clusters and in bamboo segments. Diffusion alone does not cause failure. It is the atomic flux divergence at certain sites that causes the lines to fail. Because the diffusion along the Aluminum-oxide interface is slower than along the grain boundaries, atomic fluxes inside polygranular clusters are larger than those in bamboo segments. Therefore, locations where polygranular clusters and bamboo segments join are sites of a large flux divergence [12, 13]. Atoms deplete at the upwind end of a polygranular cluster and accumulate at the downwind end giving rise to tensile and compressive stress, respectively. The resulting stress gradient, in turn, generates a back-stress force opposing

the electron-wind force. The stress in a polygranular cluster reaches a steady state stress when the two opposing forces are balanced. The maximal stress achieved is proportional to the length of the cluster. This is demonstrated in the Appendix where we present the Korhonen model for stress evolution due to electromigration in confined metal lines and discuss the utility of the one dimensional model used.

Assuming the initial stress is zero, the maximum stress $\sigma_m$associated with a current density j for a cluster of length L is given by:

$$jL=\frac{2\sigma_m\Omega}{\rho Z^* q}, \tag{2.1}$$

where is the electric resistivity, Ω is the atomic volume, Z^* is the effective charge and q is the fundamental charge. It is postulated that failure of a cluster occurs only when the maximum stress is larger than a critical failure stress σ_{cr}. For a given j and cluster of length L, if σ_m is less than the critical stress required to induce failure, σ_{cr}, the cluster can, to a first approximation of dominance of grain boundary diffusion [14],be considered as not a potential failure site. The lifetime statistics of near-bamboo lines will therefore be a function of the number of clusters longer than a critical length L_{cr}, $N_{L>L_{cr}}$, found for a given current density using equation (2.1) and taking σ_m=σ_{cr}. In such lines, where $N_{L>L_{cr}}>1$, grain boundary diffusion alone causes failure of the line through the failure of a polygranular cluster longer than L_{cr}. On the other hand, in bamboo-like lines, characterized by $N_{L>L_{cr}}<1$ (no cluster longer than L_{cr}), grain boundary diffusion alone is not enough to cause failure, and failure occurs via transgranular diffusion mechanisms.

At this point, we are able to interpret qualitatively the dependence of the median time to failure of interconnects on the ratio of their width and the median grain size w/D_{50}, already seen in figure 2.1. Starting at large w/D_{50}, as w/D_{50} decreases, spanning grains become likely but more clusters are longer than L_{cr} so that t_{50} decreases. However, as w/D_{50} continues to decrease, more grains span the width of the line, splitting the clusters into shorter ones, and it becomes more likely for cluster lengths to be less than the critical length, so that t_{50} begins to increase. As w/D_{50} becomes very small, all the clusters are shorter than the critical length and have a much better reliability. It can be concluded, therefore, that the reliability of near-bamboo lines depends strongly on the polygranular cluster length distribution in as-patterned lines.

In an attempt to quantify what has just been seen qualitatively of the effect of feature sizes and grain structure of lines on their reliability, an analytic model linking the cluster length distribution in lines to the grain structure characteristics of the film they are etched from, D_{50}, and σ_d, and the lines geometrical characteristics, width w, and length L_{tot}, has been developed [6, 7] and will be briefly outlined in the following section. Ultimately, the goal being reliability assessment, an analytic model for the dependence of failure times of lines on their grain structure and geometry characteristics via their cluster length distribution is then presented.

2.3 Analytic Model for the Microstructure of As-Patterned Lines

Grain sizes in an as-deposited film are lognormally distributed so that

$$f_D(D)=\frac{1}{\sigma_d D\sqrt{2\pi}}\exp[-(\frac{1}{\sqrt{2}\sigma_d}\ln\frac{D}{D_{50}})^2], \tag{2.2}$$

where D is the grain diameter, D_{50} is the median grain diameter, and σ_d is the lognormal standard deviation of the grain diameter (usually ranging between 0.3 and 0.6). The number of grains spanning the width w or bamboo grains can then be estimated [6] by (# per length D_{50})

$$N_b=\int_w^\infty f_D(D)\frac{w-D}{w}dD. \tag{2.3}$$

By accounting for the probability of adjacent spanning grains, the number of polygranular clusters can be estimated as

$$N_p=N_b[1-(\frac{L_b}{L_{tot}})^2], \tag{2.4}$$

where L_b and L_{tot} are respectively the total length of the bamboo segments and the total length of the line, and L_b is given by

$$L_b=L_{tot}(\frac{\pi}{4}\int_w^\infty f_D(D)\frac{D-w}{w}DdD)/L_{tot} \tag{2.5}$$

and

$$L_{tot}=\frac{\pi}{4\omega}\int_w^\infty f_D(D)D^2dD. \tag{2.6}$$

The average polygranular cluster length is thus given by

$$\bar{L}_p=(L_{tot}-L_b)/N_p. \tag{2.7}$$

These expressions for N_p and $\bar{L}_p$ given above have been tested for lines of different widths patterned from simulated structures with lognormally distributed grain sizes, such as the one shown in figure 2.3. The predicted and measured values were found to be in very good agreement, as shown in figure 2.4.

Although the distribution of cluster lengths has been found to be lognormal [6], its tail for long clusters can be approximated by an exponential distribution so that

$$f_c(L)=\frac{N_p}{\bar{L}_p}\exp(\frac{-L}{\bar{L}_p}), \tag{2.8}$$

and so that the number of clusters longer than a critical length is given by

$$N_{L>L_{cr}}=\int_{L_{cr}}^{\infty} f_c(L)dL=N_p\exp(\frac{-L_{cr}}{\bar{L}_p}), \tag{2.9}$$

where N_p and $\bar{L}_p$ are determined as a function of L_{tot}, w, D_{50} and σ_d using equations 2.3-2.7.

This model allows the prediction of $N_{L>L_{cr}}$ as a function of the line geometrical characteristics and the film grain structure but also the current density since L_{cr} is linked to j through the value of (jL_{cr}) fixed by equation 2.1 (the experimentally observed value of this product is around 1000 A/cm). This in turn has two major applications. First, it can be used to determine the limiting values (w^*, j^* or $L_{tot}{}^*$) separating the case of dominance of transgranular failures ($N_{L>L_{cr}}<1$) from the case of dominance of grain boundary diffusion failures ($N_{L>L_{cr}}>1$). For example, the value of j^* below which

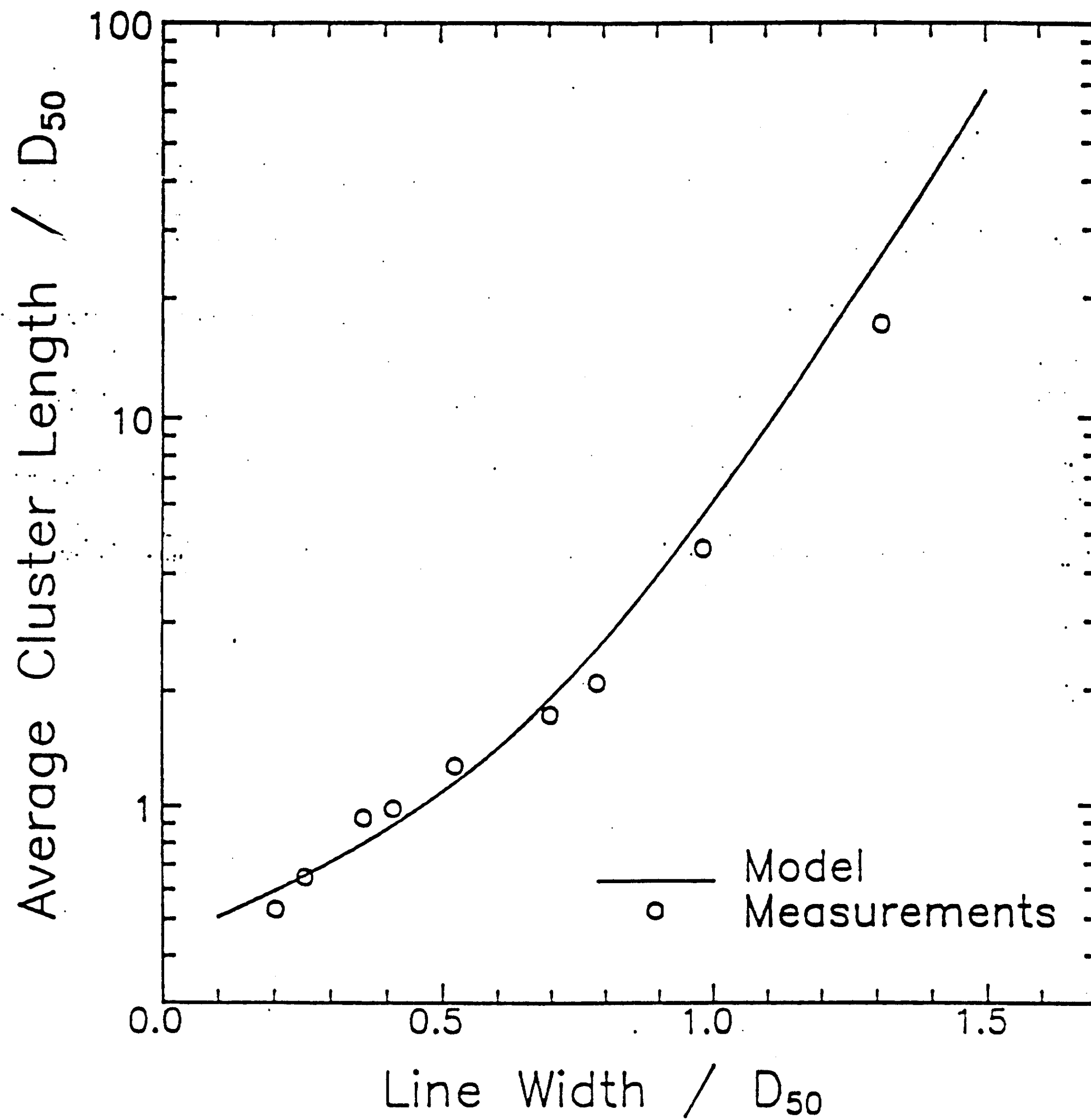

Figure 2.4 The predicted and measured average cluster lengths as a function w/D_{50}. Predicted averagew lengths from ther model match the measured values well.

transgranular mechanisms are expected to dominate will be a function of L_{tot}/D_{50}, w/D_{50}, and σ_d, and is calculated usually using an experimentally determined value of (jL_{cr}). Using (jL_{cr})=1000 A/cm, the calculations of j^* vs w/D_{50} for different values of L_{tot}/D_{50} are shown in figure 2.5. For a given L_{tot}/D_{50}, the region below the curve obtained corresponds to values of j and w/D_{50} for which bamboo-like failure mechanisms are expected, whereas the region above it corresponds to the case of dominance of grain boundary diffusion failure mechanisms.

The microstructure model can also be used, in conjunction with a simple failure model, to determine the reliability of lines in the case $N_{L>L_{cr}}>1$ where grain boundary diffusion controls failure. This model is discussed in the following section.

2.4 Analytic Model for As-Patterned Near-Bamboo Lines Reliability

We can use the failure unit model [8, 15] to calculate the median time to failure of near bamboo-lines. In, this model, a polygranular cluster can be considered to be a single failure unit having failure characteristics characterized by a lognormal cumulative failure distribution function, $F_i(t, L_i)$. An entire near-bamboo line can be considered as a series of these units. The cumulative failure distribution function (cdf) of a line, or equivalently the probability of failure before time t, G(t) is then

$$G(t)=1-\prod_{i=1}^{N_s}[1-F_i(t,L_i)], \qquad (2.10)$$

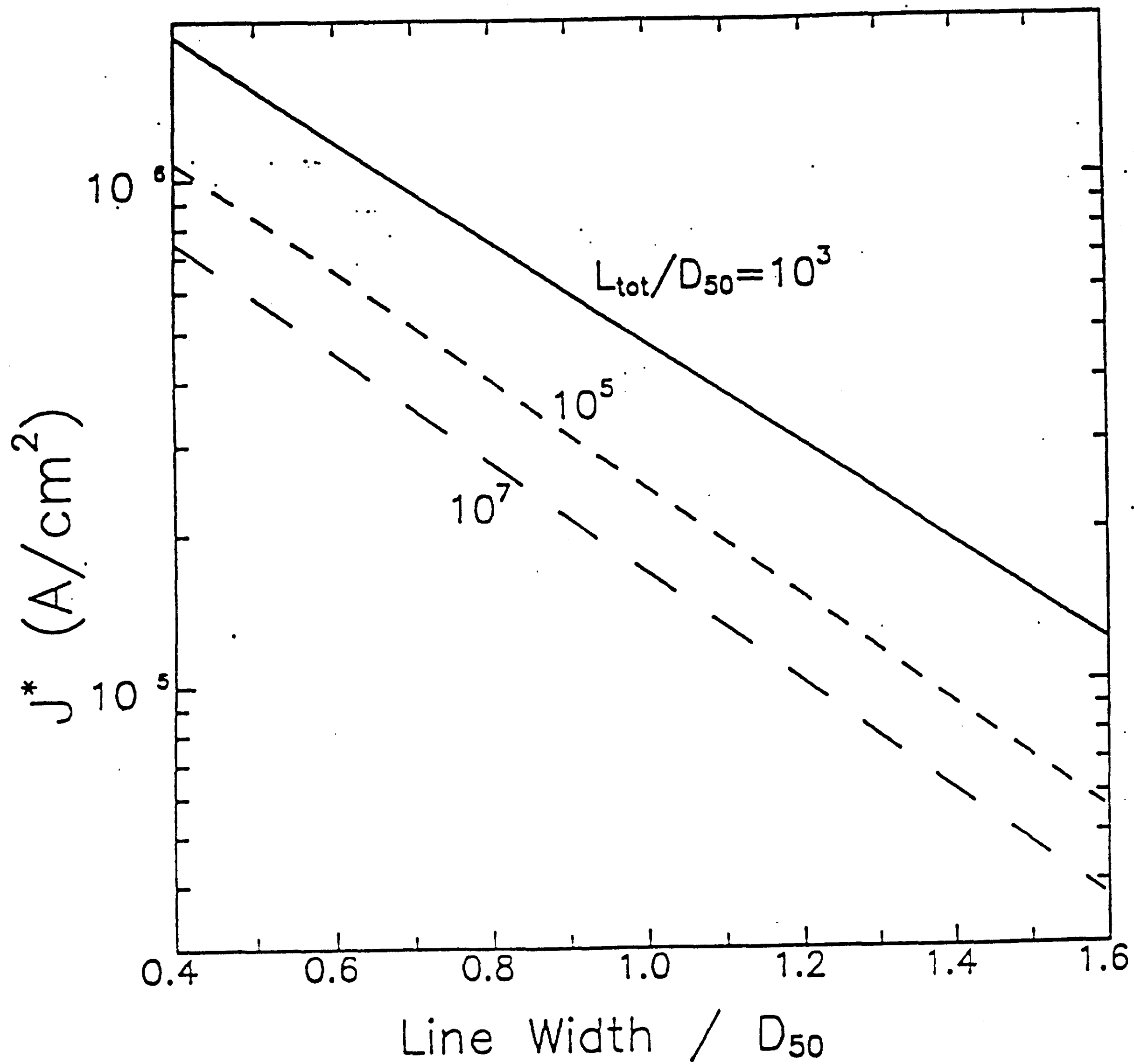

Figure 2.5 The transition current density, j^*, dependence on w/D_{50}. Different lines represent different total line lengths, L_{tot}/D_{50}.

where N_s is the number of units in series or, in this case the number of polygranular clusters [8, 16, 17]. In a first-order model we can assume that clusters shorter than the critical length don't fail, and that the cdf of clusters longer than L_{cr} are the same, $F_i(t, L_i)$=$F_c(t)$ for any length L_i greater than L_{cr}. In this case, the failure probability of a population of lines obeys the following equation

$$G(t)=1-[1-F_c(t)]^{N_{L>L_{cr}}}, \tag{2.11}$$

where $N_{L>L_{cr}}$ is predicted by the microstructure analytic model (equation 2.9).

Figure 2.6 shows the median time to failure predicted using this model for a population of lines with given values for w/D_{50}, σ_d, and L_{tot}/D_{50}, as a function of the current density j. We assumed that $F_c(t)$ is the cdf for a lognormal probability density function, with $t_{50,c}=10^5$ hours and variation σ_c=1.5. This result shows that at high current densities $\ln(t_{50})$ is proportional to j^{-2},as is assumed in Black's analysis. However when j decreases, L_{cr} increases leading $N_{L>L_{cr}}$ to decrease, and t_{50} increases more rapidely than j^{-2}. In near-bamboo interconnects, the j^{-2} dependence is therefore expected only when $N_{L>L_{cr}}>>1$. When $N_{L>L_{cr}}<1$, bamboo-like mechanisms dominate and the dependence on j is not completely assessed. The transition from near-bamboo to bamboo-like behavior may occur between test conditions and service conditions, in which case lifetime projections based on test result may be very conservative.

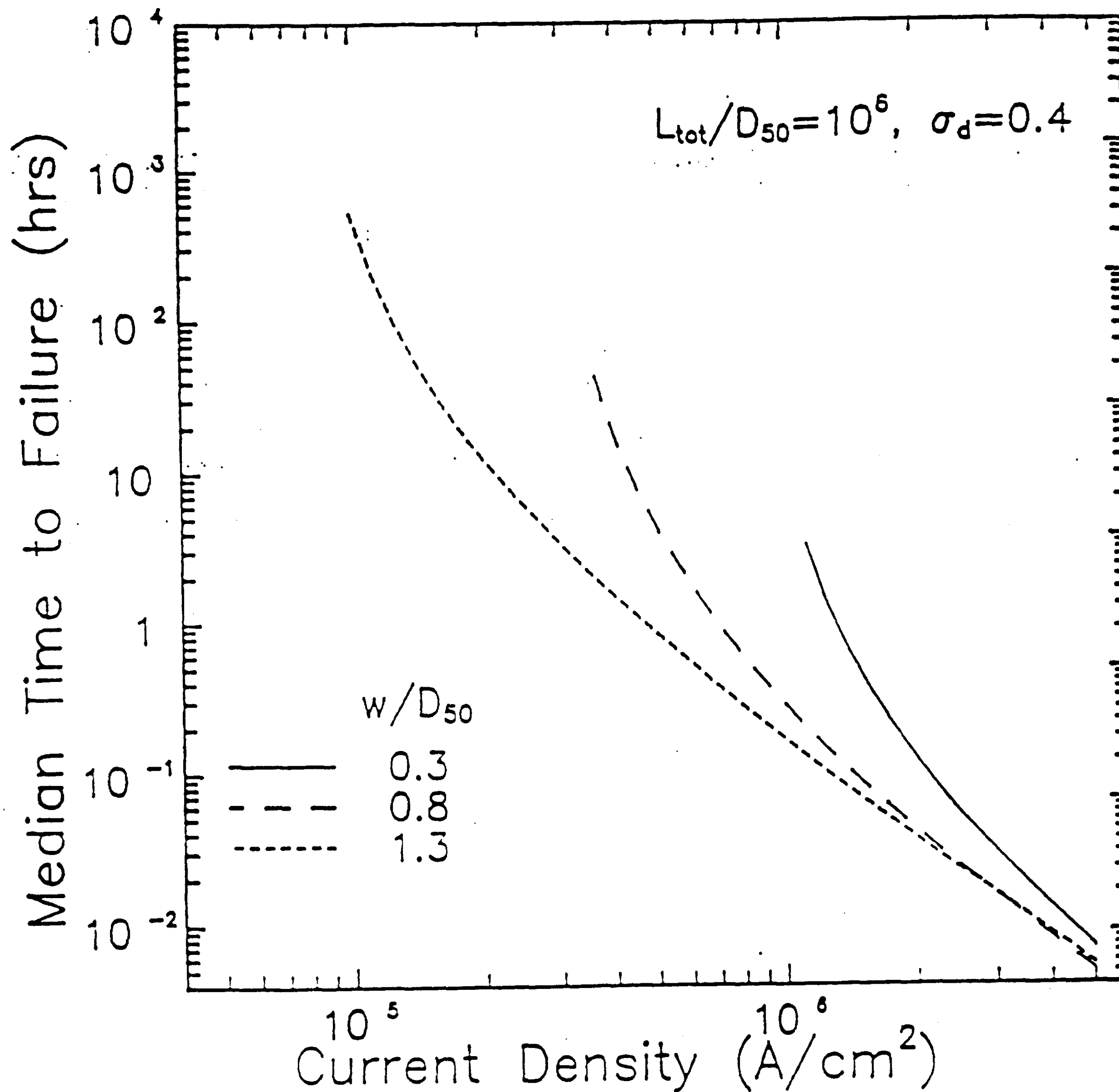

Figure 2.6 The expected dependence of the median time to failure, t_{50}, on the current density j for the polygranular failure mechanism. Projection to lower densities requires experimental results for transgranular failure mechanisms

Figure 2.7 shows t_{50} calculated as described above as a function of w/D_{50}, given σ_d, L_{tot}/D_{50}, and j. This prediction matches the observations discussed in association with figures 2.1 and 2.3.

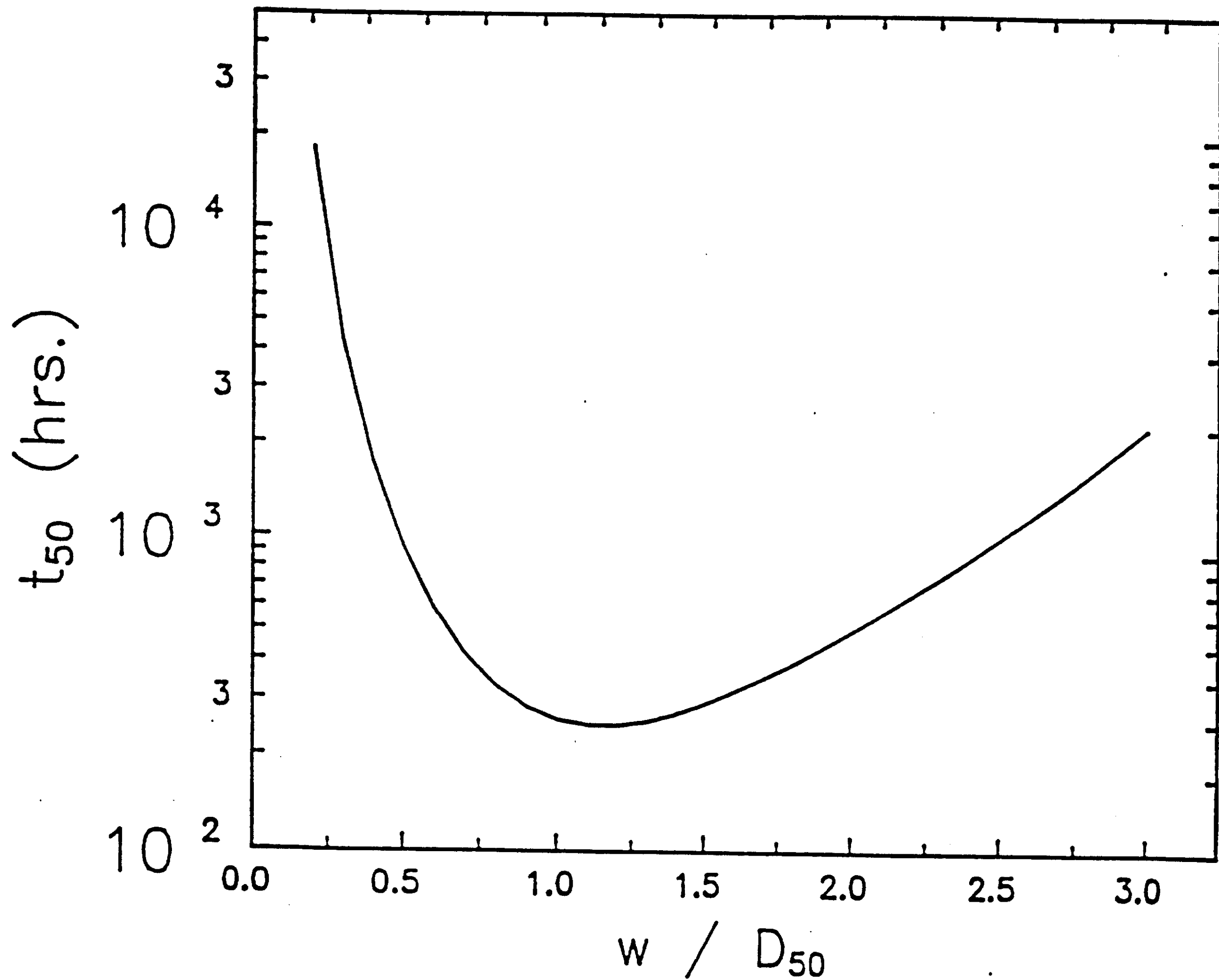

Figure 2.7 Predicted dependence of t_{50} on w/D_{50}.

2.5 Evaluation of the Previous Models and their Limitations

The simple model outlined above predicts the lifetime of interconnect lines in the near-bamboo regime in a more accurate way than the conventional scaling methodology since it takes into account both the geometrical parameters of a line and the statistical microstructural characteristics of the film the line is etched from. The predicted behavior matches well the experimentally observed one and the method allows a less conservative reliability assessment than the one done assuming all lines have the worst-case width and length.

However, this model, in its simplicity, is subject to several limitations. The model is limited to the case in which failure occurs within a cluster through grain boundary diffusion alone and in which bamboo diffusion is neglected. While this is probably the case at test conditions since the current densities used are high, at service conditions, where current densities are lower, transgranular diffusion mechanisms are no longer negligible, and interaction between clusters [18, 19] may lead to failure even though all clusters are shorter than the critical length. An analytic model assessing these effects would allow a better extrapolation of the test results to service conditions. Also, the model described above predicts the reliability of as-patterned lines and does not account for the beneficial effects of the post-patterning annealing and accompanying grain structure evolution that occurs during high temperature processes such as passivation. Finally, the model handles flat straight lines interconnects, while actual interconnects

have various geometries. A microstructure model, similar to the one developed for straight lines, for interconnects of different shapes is important for a more realistic assessment of their reliability.

Chapter 3

Simulation Package and its Modification

3.1 The Simulation Package

The dependence of the electromigration behavior of interconnects has been established, it has been quantified for flat straight interconnect lines as a function of the line width and length as well as the statistical microstructural characteristics of the film the line is etched from and the current density information. In order to assess the behavior of interconnects with more general geometries, we need an understanding of the microstructural characteristics of such features. This can be done, similarly to the case of straight lines, by generating large populations of interconnects with given geometrical characteristics and establishing the relation between these geometrical characteristics and the statistical microstructural characteristics of those features. I have developed a new patterning routine *pattern* makes it possible to use the grain growth simulation package to simulate such populations. The *pattern* program is designed to take a continuous film grain structure generated by the grain growth program and pattern it to obtain the desired pattern shape. We will now discuss the simulation package and the newly introduced capacity.

The simulation package is made up of six computer programs. It is made of approximately 20,000 lines of executable C code. The programs *nucleate, impinge*, and

gb_init generate the nucleation and growth to impingement structures used to initiate grain growth simulations. The patterning of continuous film structures into thin film strips is performed by *etch*. The patterning of continuous film structures into more general shape patterns is handled by the new routine *pattern*. The program *anneal* simulates grain growth in both continuous films and thin film strips and is currently being extended to handle grain growth in patterned structures with arbitrary shapes.

The *nucleate* and *impinge* programs generate the Johnson-Mehl [23] continuous nucleation structure. This structure results from the nucleation and growth-to-impingement of grains on a two-dimensional surface. Here, grain nucleation (at random sites) continues at the same time as the growth of previously nucleated grains occurs. In other words, grain nucleation occurs continuously throughout the growth-to-impingement process. Throughout this process, the probability of grain nucleation within a unit of untransformed area remains constant. In the fully impinged structure, each grain boundary is a segment of a hyperbola. We generate the Johnson-Mehl structure via a three-step process. First, *nucleate* establishes a collection of nucleation sites, shown as dots in figure 3.1. The program *impinge* then determines the positions of the grain boundary triple junctions and also specifies arrays of points to represent the grain boundaries. We refer to the points describing the grain boundary triple junctions as triple points. The points representing the grain boundaries are called segment points. A third program, *gb_init*, is then used to convert the bare-bones representation of the grain structure generated by *nucleate* and *impinge* into the linked data structure recognized by *etch*, *pattern*, and *anneal*. Periodic boundary conditions are used within all of the five

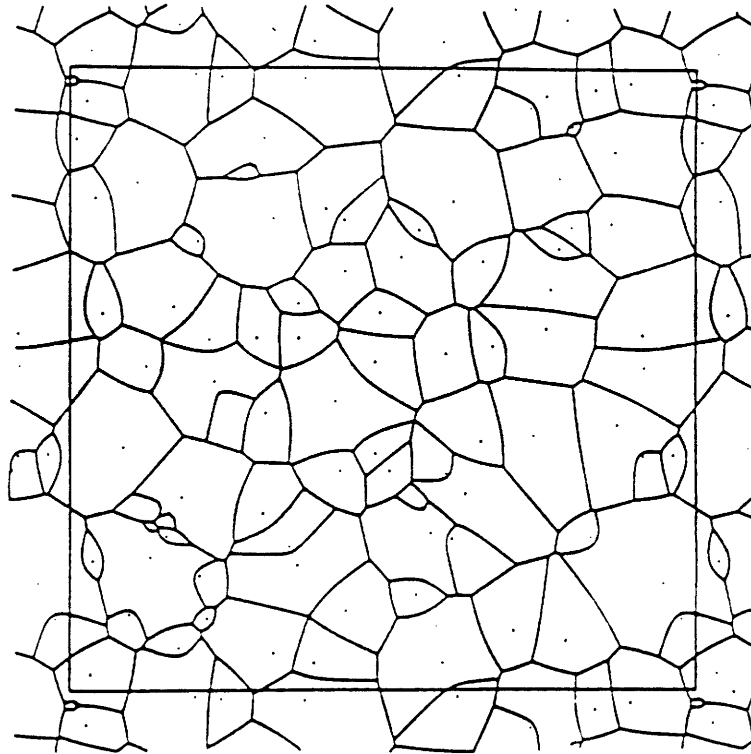

Figure 3.1. The Johnson-Mehl structure generated by the programs *nucleate* and *impinge*. The dots represent grain nucleation sites.

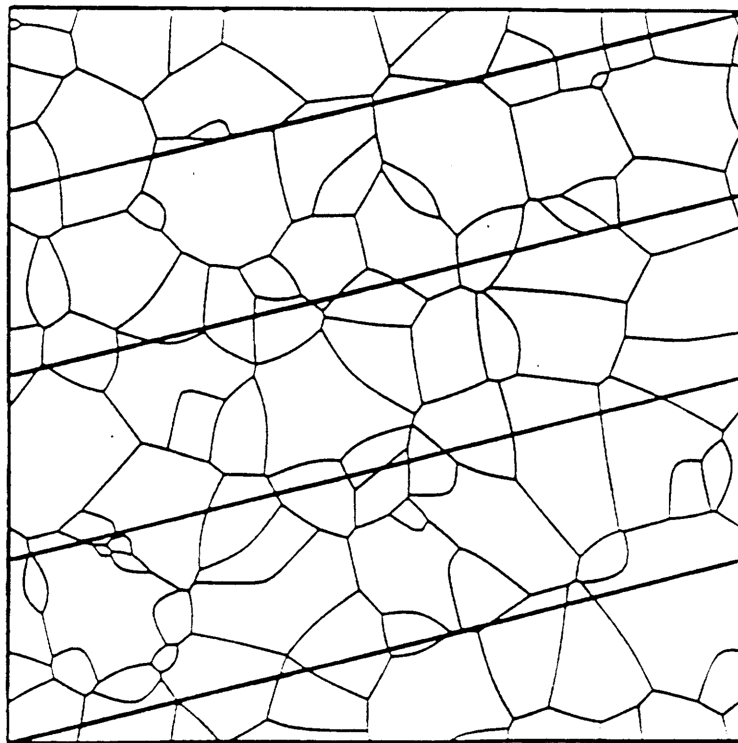

Figure 3.2. Patterning lines used by the *etch* program. These patterning lines will convert the continuous film into a single, thin film band.

previously developed programs in the simulation package. The Johnson-Mehl structure of figure 3.1 clearly demonstrates these boundary conditions. Here, grains located at the array's lower edge are duplicated at the upper edge, those at the left edge are also found at the right edge, etc. The resulting 2-D grain structure may be envisioned as the surface of a torus.

The *etch* program is designed to convert an entire continuous film grain structure into a single strip structure. In figure 3.2 we show an example of lines used to perform this task. Each line in the figure represents both the top edge of the lower strip slice and the bottom edge of the upper slice. During the patterning process, a grain boundary which traverses the etch line is broken into two segments. Each of the two segments is terminated at a new triple point inserted on the appropriate strip edge. Notice that due to periodic boundary conditions, the strip actually wraps back on itself, forming a closed loop, or band. To operate the *etch* program, one specifies the input structure and the desired number of slices. The input structure may either be the nucleation and growth-to-impingement structure, created by the sequence *nucleate-impinge-gb_init*, or a structure resulting from a period of continuous-film grain growth, as produced by *anneal*. The number of slices determines the width of the strip: $w=a/\sqrt{n^2+1}$, where a is the side length of the square simulation array and n is the number of slices. Also, since the total area of the film is conserved, the total strip length l is: $l=a^2/w=a\sqrt{n^2+1}$

3.2 Generation of Interconnects with Various Geometries

The *pattern* program, which I have written and recently incorporated to the simulation package, provides the possibility of patterning the film with any general shape polygon. A direct generalization of etch to achieve this goal was impossible because etch constantly uses the periodic boundary conditions of the film and also produces a stripped structure with the same periodic boundary conditions. Here, as in real interconnect designs, the pattern is general and does not have any periodic boundary conditions, and therefore the periodic structure of the film cannot be used to simplify the patterning algorithm. In figure 3.3 we show the result of the patterning of a film with two very commonly found interconnect elements, an L-element in figure 3.3.a, and a T-element in figure 3.3.b. The program begins by finding all the intersection points between grain boundaries and the edges of the polygon to be patterned. These intersection points are then sorted on the edges of the pattern in a counter-clock-wise order. The process of incorporating these new points as well as the points representing the corners of the pattern as part of the linked data structure then begins. It involves starting at one intersection point and walking from one intersection point to the following in a counter-clockwise way on the polygon edges, making the new edge triple point incorporations, creating new grains due to the splitting by the edge, and updating the links of the data-structure. Eventually, one returns to the intersection point of departure, having transformed the continuous film into two structures, the inner pattern, and also the outer one, which also

(a)

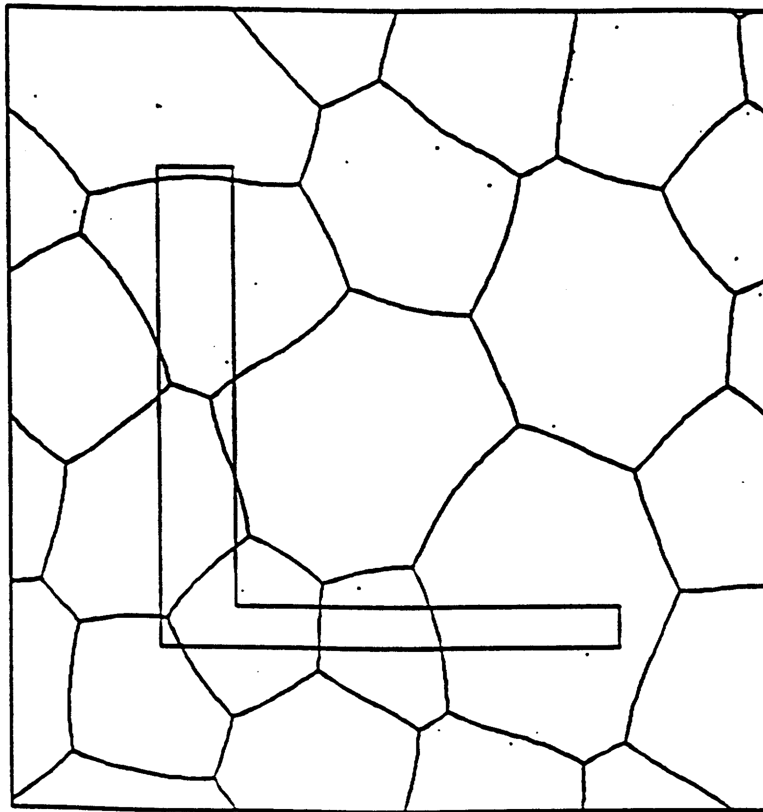

(b)

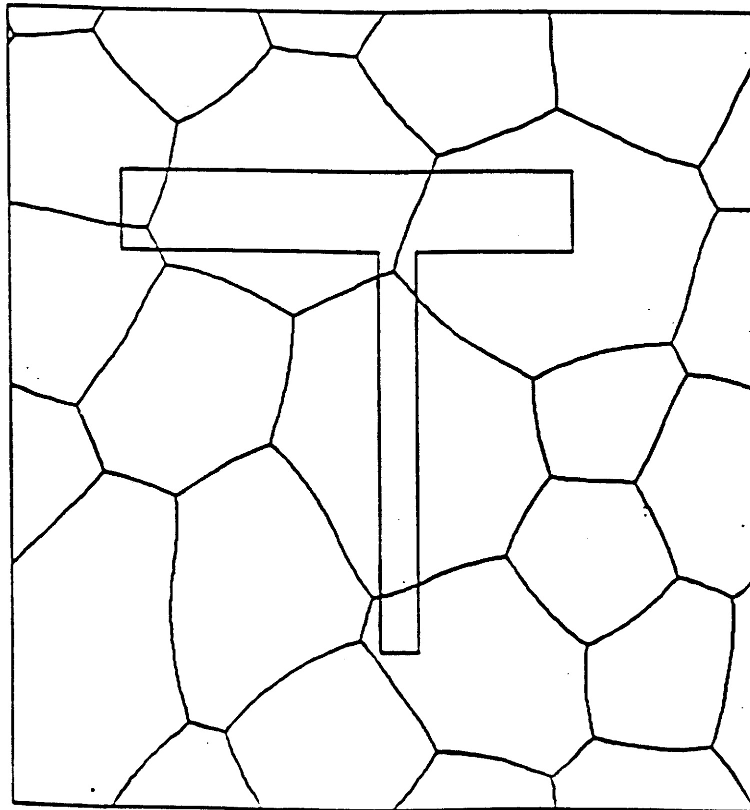

Figure 3.3 (a) Patterning an L structure using the program *pattern*, (b) patterning a T structure with the same program.

could be an interesting feature to analyze. In fact one other reason of keeping the outer structure is to make only the minimum necessary changes in the initial data structure. The simulation package represents the grain structure in such a way that each boundary point and triple point is linked to points which are its nearest neighbors. Using this linking information, it is possible to move from one point to its neighboring point, then to a point neighboring this second point, etc. By this process one can walk along the linked grain boundary network. In figure 3.4 we show a close-up view of the patterning process. At an intersection point (i) between the grain boundary and the edge, two new edge triple points are inserted, one internal (as part of the inner structure), and one external (as part of the outer structure). As part of the insertion process, the links between boundary points straddling the etch line are broken, and then reformed with the new appropriate edge triple point. Also, the newly created edge triple points are linked to the two previous ones, thereby defining segments of the pattern side-wall. After this is done, the program walks around the grains in a counter-clock-wise way until it reaches the next intersection point (i+1). The grain split in two by the edge portion [i, i+1] is identified and a new label for the created external grain is inserted (the internal grain keeps its original label). Also grain neighbors are updated in a consistent way. The corners of the pattern are inserted in the data structure as new stagnant segment points. The insertion process is continued in this manner until the program returns to the starting point of the process. The particular case of a lense, which is a grain with only two grain boundaries, presents more complicated technical issues because of the nature of the data structure itself. This case has been dealt with, but since its interest is purely technical, it has been omitted here,

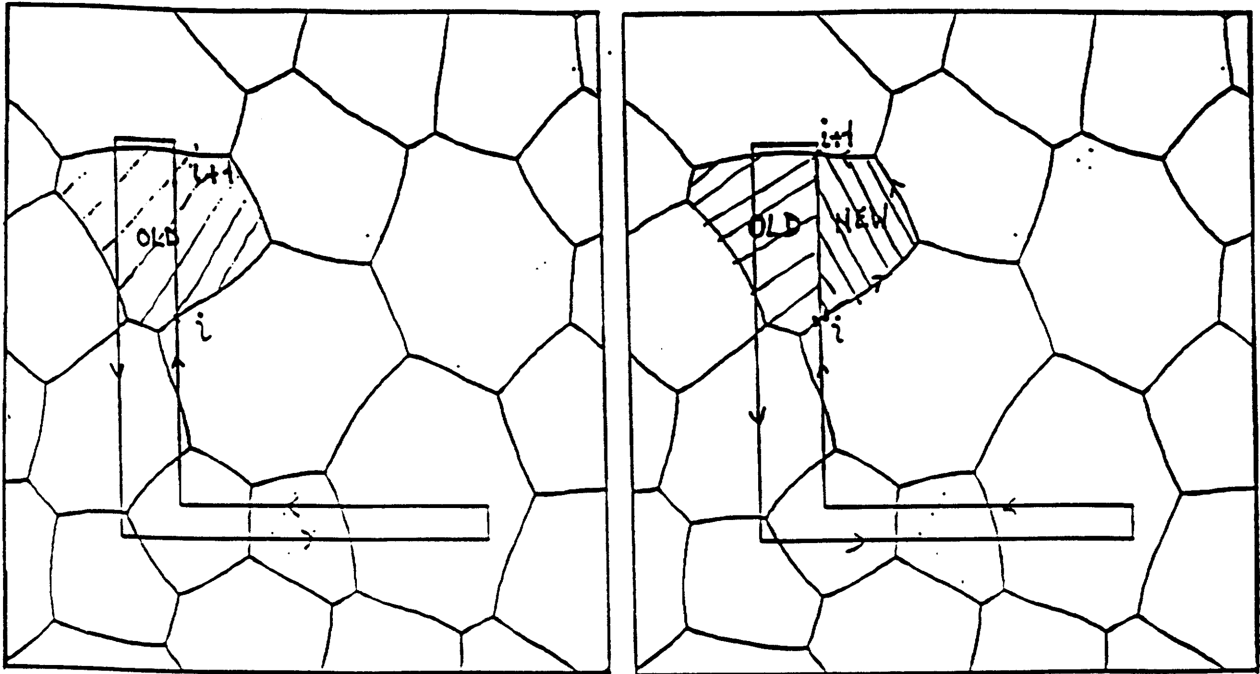

Before

- 1 grain Old
- no edge triple point at location i
- no stagnant segment point at corners

After

- 2 grains Old and New
- new edge triple points
- new stagnant segment point created in case of a corner
- links created for new triple points
- links created for new grain
- links updated for triple points defining New

Figure 3.4 Schematic illustration of the patterning algorithm used by the program *pattern*. The routine repeatedly takes the next edge triple points couple, establishes the links with the previous ones, as well as their surrounding neighbors. It also creates a new external grain and updates its links.

along with many other technical details.

The *anneal* program models 2-D grain growth in both continuous films and thin film strips resulting from *etch*. The program simulates grain growth by alternately moving a structure's grain boundaries and repositioning its triple points. The theory behind this involves the fact that grain boundary velocity is proportional to local curvature. Generalizing the routine to simulate grain growth in general patterns is one of the major future tasks.

Chapter 4

Structure Statistics

4.1 End Effects on Microstructure Statistics of Straight Lines

The newly developed patterning routine allows more flexibility than the one developed in *etch*. Apart from its major advantage of providing the possibility of etching generally shaped polygons, it can also be used in the particular case of a rectangular pattern to simulate finite length straight line structures. By etching a single strip from a film using the *etch* program and patterning it using *pattern* with many lines having the same cumulative total length as the strip and all having the same width as the strip, one can compare the microstructural characteristics obtained in the two cases and assess the end effects resulting from the fact that the lines now have finite lengths. Figure 4.1 presents the results obtained in the two cases for the polygranular cluster length distribution. In light of these results, it appears that, as expected, the end effects are negligible as long as the ratio of the finite line length to the line width is reasonably high (in the presented case it is of about 85). In contrast, as this ratio becomes smaller, the difference between the statistics of the semi-infinite line in comparison with the equivalent set of finite ones is expected to increase, as more long clusters are shortened because of end effects. Not only are we able to simulate these divergences, in a similar manner as done for longer finite lines, but also, with a correct knowledge of the cluster

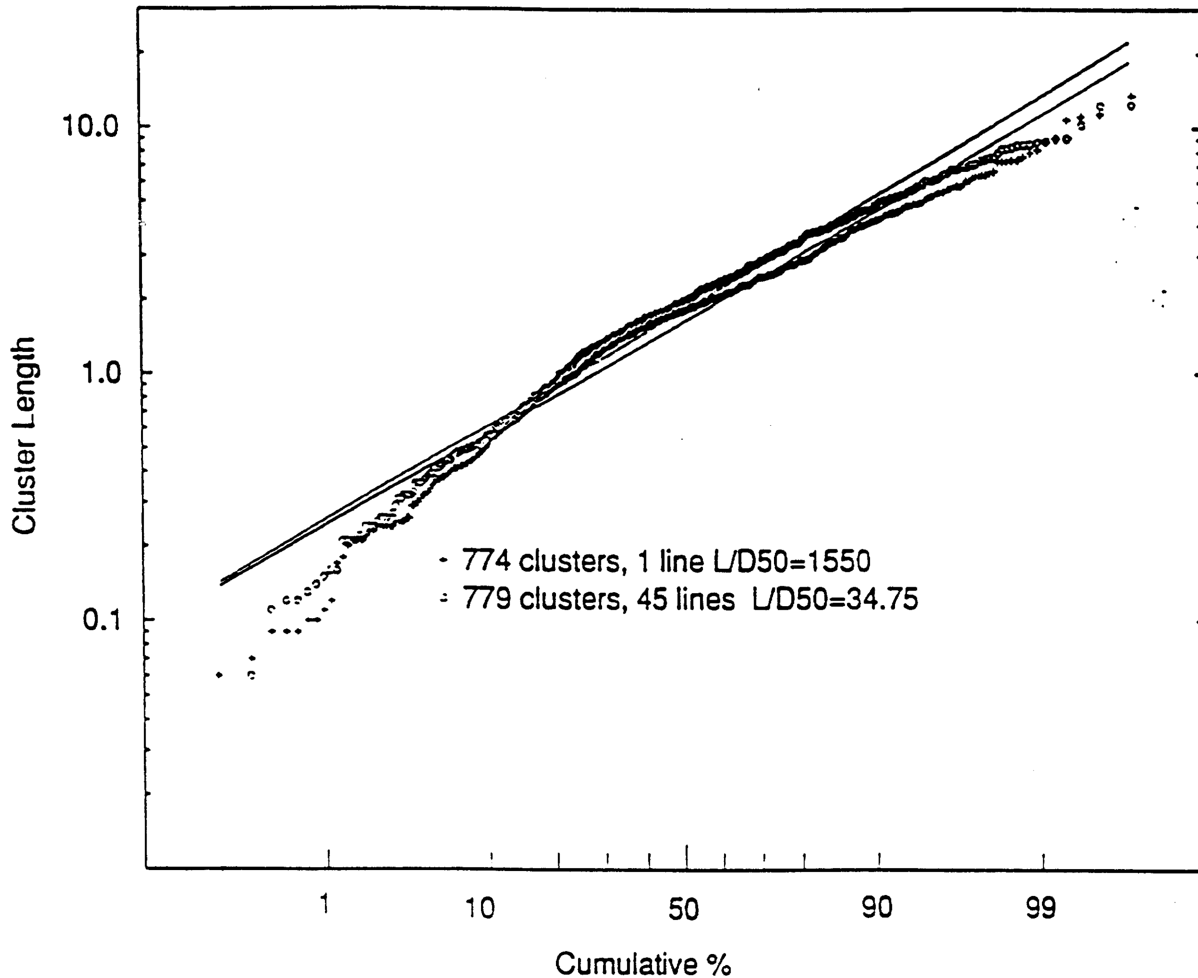

Figure 4.1 End Effects on Microstructure statistics. Lognormal plot of cluster length distribution in 2 cases, (1) 1 semi-infinite line (L_{tot}/D_{50}=1550, W/D_{50}=0.41) etched with *etch*, and (2) a collection of 45 lines with the same width, and with finite length (L/D_{50}=34.75, this gives the same total length) etched with *pattern*. In this case where the length of the finite lines is relatively large compared to the line width (L/W=85), the difference observed is negligible.

length distribution we can analytically quantify these end effects simply by evaluating the proportion of clusters terminated due to the edges. That is one of the motivations for investigation of the distribution of polygranular cluster lengths as well as the distribution of bamboo segment lengths, in order to come up with a reliable analytical model for the line microstructures, as we will see in the next section.

It is important to note, however, that the matching results between the statistical microstructural characteristics obtained on one hand for semi-infinite line using the etch routine and on the other hand for an equivalent set of relatively long finite lines using the newly developed pattern program provides us with a successful test for the accuracy of this new program.

4.2 Bamboo Length Distribution / Cluster Length Distribution

We have previously seen that a first order assessment of the reliability of straight line interconnects when subjected to electromigration requires the knowledge of the polygranular cluster length distribution in a line. More precisely we have seen that only clusters longer than a critical length will affect the line reliability in the model used. Therefore we were only interested in the cluster length distribution, and more precisely, the tail of this distribution for long clusters that has been described by an exponential distribution function. A more accurate assessment of straight-line reliability should not assume that only clusters longer than a critical length can fail, and the major reason for

that is that cluster interaction, which depends strongly on the inter-spacing of clusters, or equivalently the length of the bamboo segment lying between two clusters, can lead to significant diffusion through the lattices or the interface with the substrate, yielding transgranular failure mechanisms. A major step towards a more accurate prediction of straight line reliability is therefore capturing the statistics of the bamboo length distribution along the line.

In an attempt to quantify the bamboo length distribution by means of a reduced set of parameters, we have tried fitting it to a lognormal distribution, as done previously for clusters, but a deviation from lognormality is noticed for short and long segments, causing a high value for the standard deviation of the residual obtained with a linear regression (figure 4.2 and Appendix B). Remembering that in the case of polygranular clusters, the exponential distribution provided an acceptable 1 parameter statistical model, we tried to generalize the approach for the case of bamboo segments by the means of a 2 parameter statistical model provided by a Weibull distribution. The results were more satisfying, for a wide range of line-width to median-grain-size ratios w/D_{50}, going from 0.1 to 1.0, the bamboo length distribution is much better described by a Weibull distribution as we can see in figure 4.3 (See Appendix B for more details on the Weibull plot). The residual standard deviations of the linear regression are about an order of magnitude smaller in this case than the ones observed using the lognormal distribution model. The error gets smaller as the ratio w/D_{50} increases. The Weibull parameters alpha and beta are plotted as a function of the ratio of the width to the median grain size of the film, w/D_{50}, in figure 4.4. The parameter alpha, which is proportional to

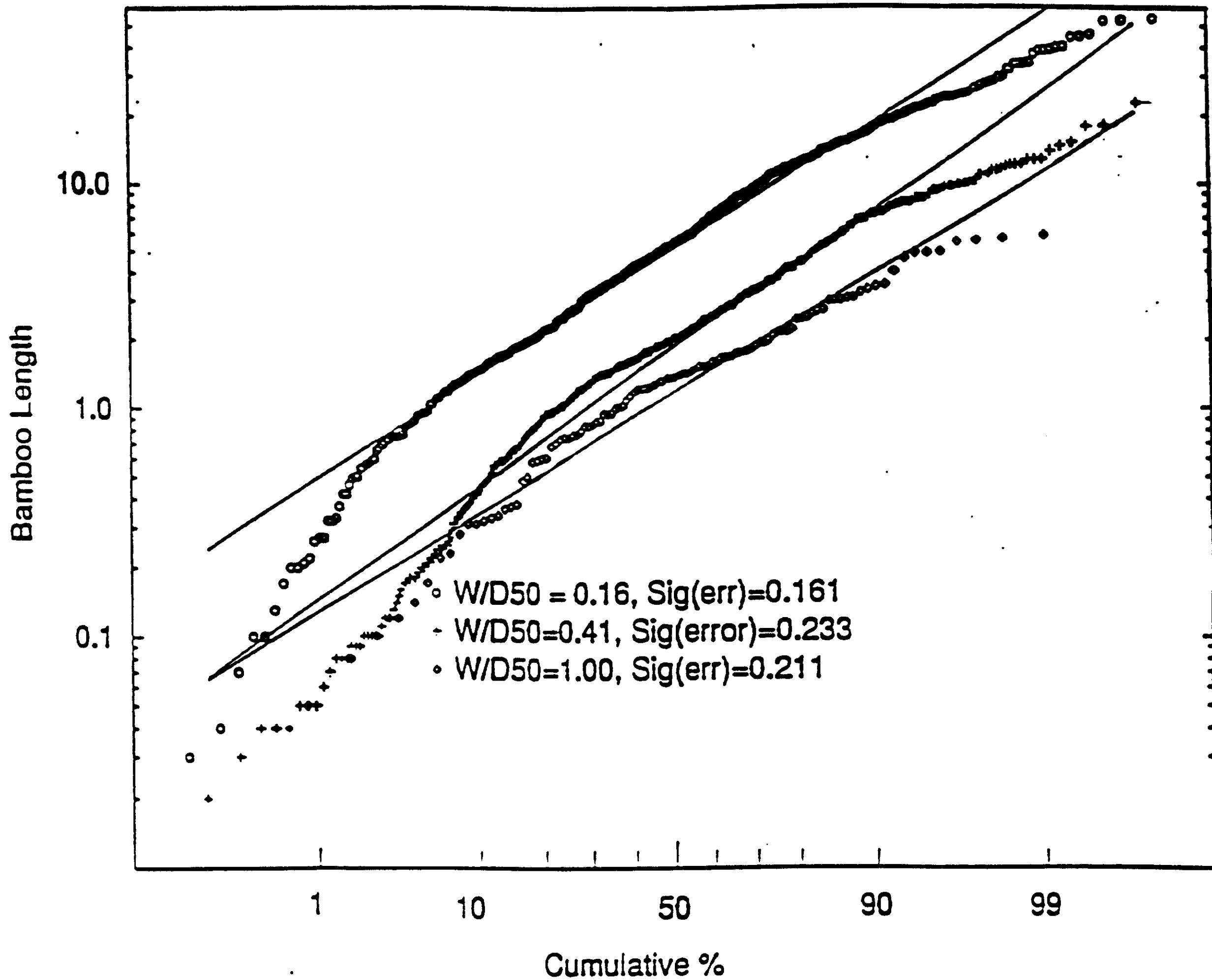

Figure 4.2 Lognormal Plot of Bamboo Length Distribution. The film structure is characterized by D_{50}=2.59, σ_d=0.28. The deviation of the residual observed is about 0.2.

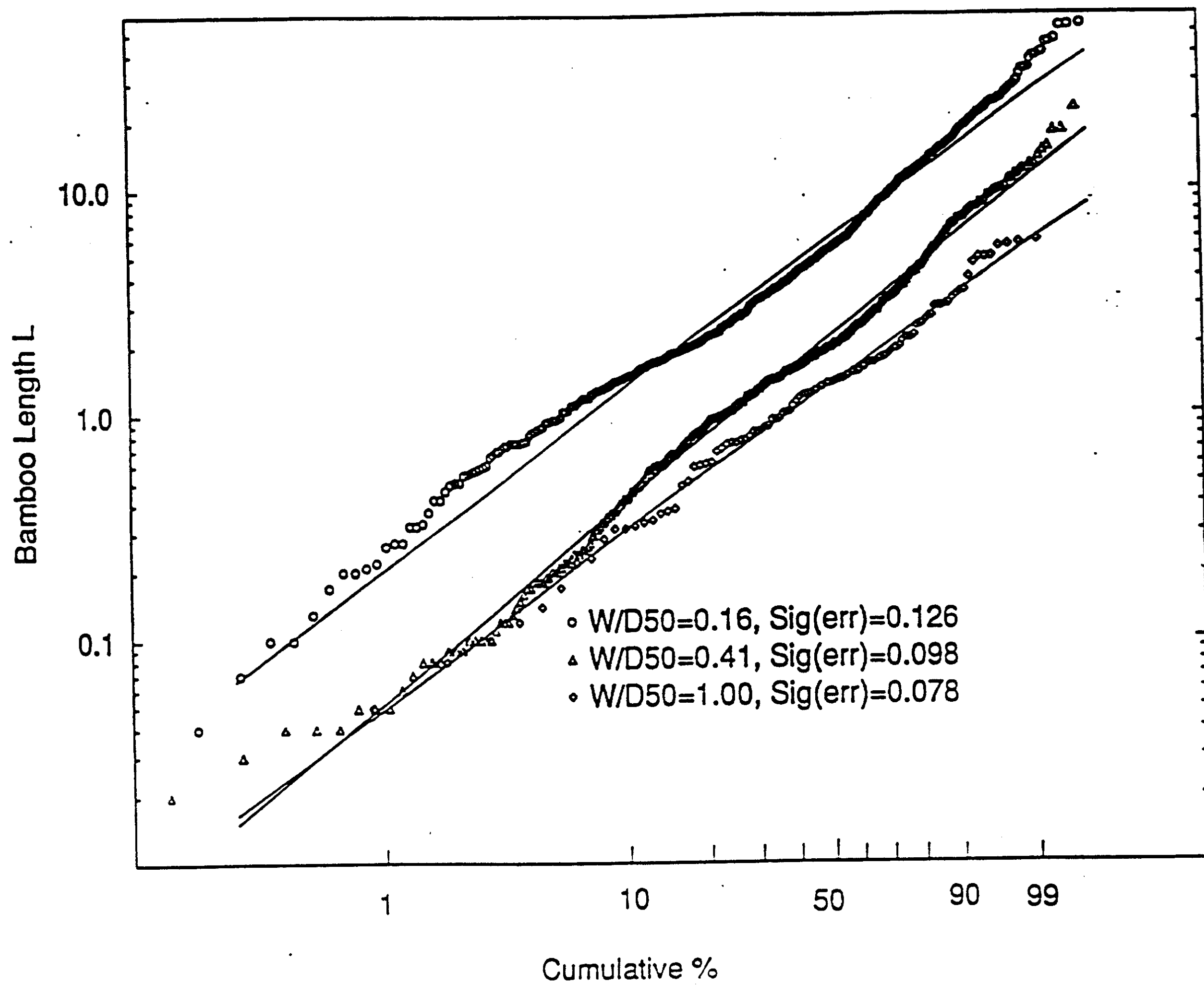

Figure 4.3 Weibull Plot of Bamboo Length Distribution. The residual standard deviation is here smaller by an order of magnitude than the case of a lognormal fit

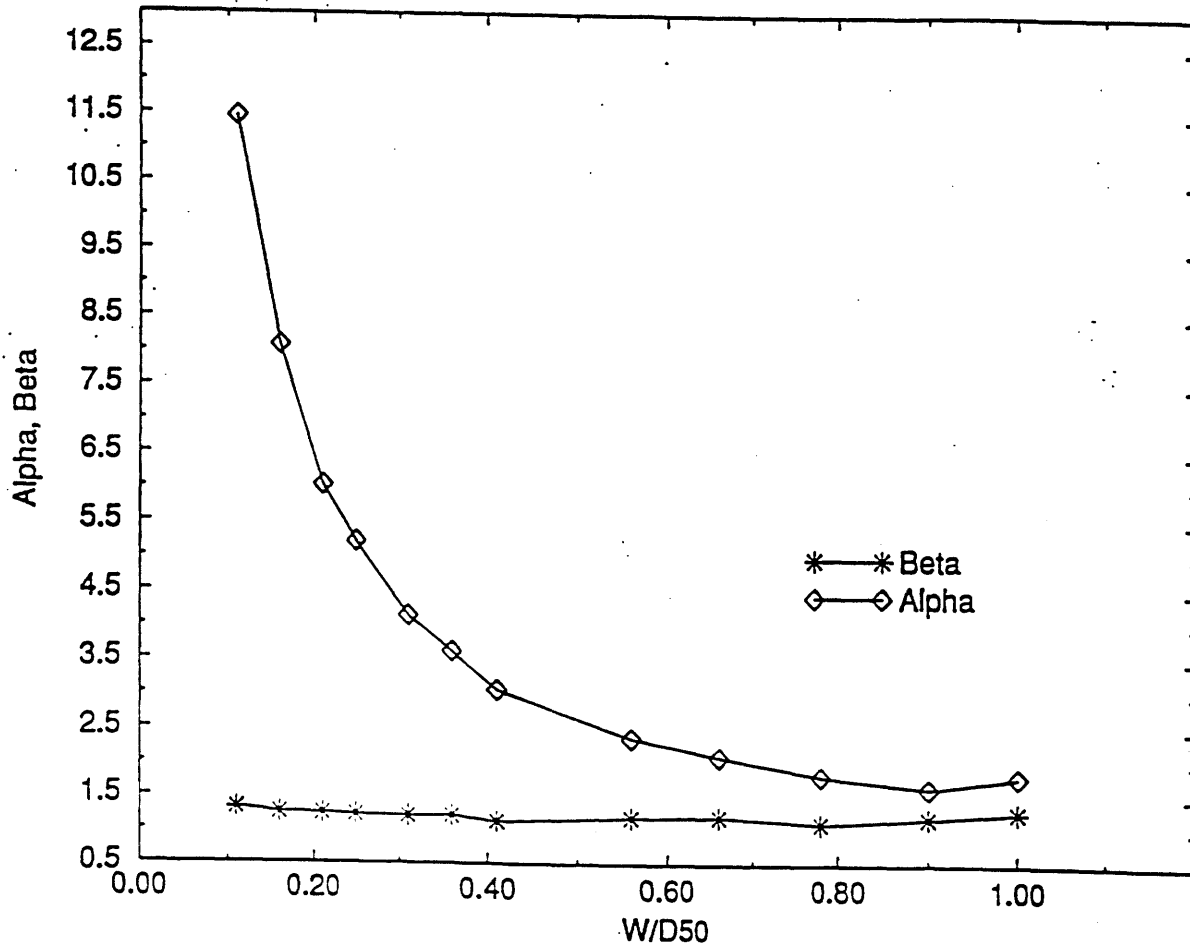

Figure 4.4 W/D_{50} dependence of the Weibull parameters in the case of the Bamboo Length Distribution. As expected, α, which is proportional to the average segment length. decreases with increasing W/D_{50} while β has an almost constant value of 1.2.

the median bamboo segment length (see equation B.7), decreases with increasing w/D_{50}, as expected. Beta on the other hand is almost independent of that ratio of w to D_{50} and has an average value of 1.2. If one notices that exponential distributions are a particular case of Weibull distributions with beta=1 then the approximation of exponential distributions for bamboo segments can also be justified.

These results have lead us to revisit our conclusions concerning the polygranular cluster length distribution. A comparison between a lognormally based vs a Weibull based linear regression shows that for small values of w/D_{50}, $w/D_{50}<0.5$, the Weibull distribution better describes the cluster length distribution, whereas for higher values of w/D_{50}, the lognormal distribution is still a more accurate approximation (figure 4.5). However in the case of bamboo length distributions, we have seen that the Weibull distribution fits better than the lognormal distribution for a wide range of line-width to median-grain-size ratios w/D_{50}, going from 0.1 to 1.0, as shown by figure 4.6.

At this point it is worth pointing out a major potential application of these results. Knowing the distribution of cluster and bamboo segment lengths, and more precisely, knowing the dependence of the determining statistical parameters on the geometrical characteristics as well as the film microstructural statistical characteristics (as seen in figure 4.4 in the case of bamboo segments) one can use this information to generate lines with realistic microstructural characteristics without having to actually go through the grain growth simulation. Those structures can then be used as input for an appropriate reliability assessment tool as we will see in the next section.

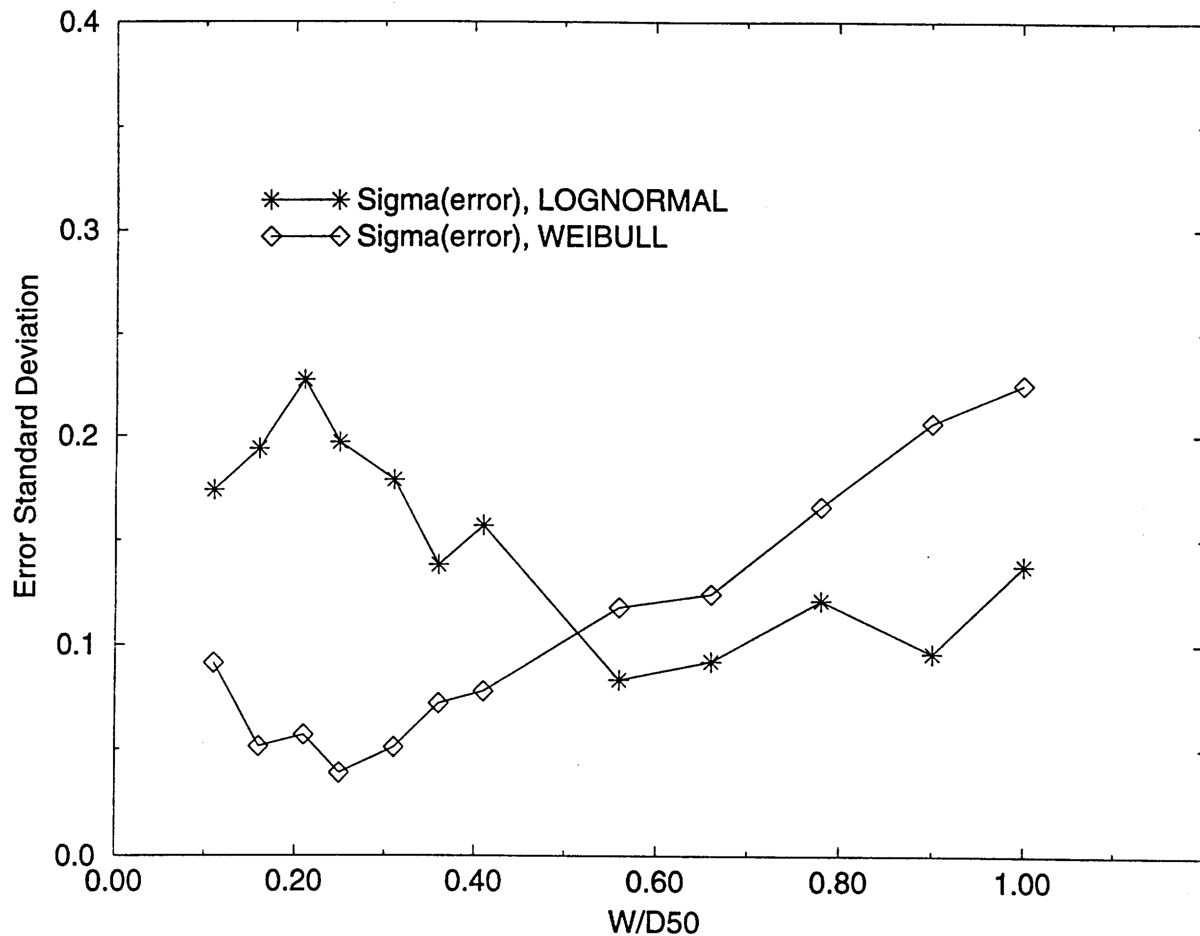

Figure 4.5 Comparison of the error in fitting a lognormal distribution vs a Weibull distribution in the case of clusters. While the Weibull distribution seems to describe well the distribution for small values of W/D_{50} (less than 0.5), the lognormal distribution fits better for wider lines (W/D_{50} more than 0.5).

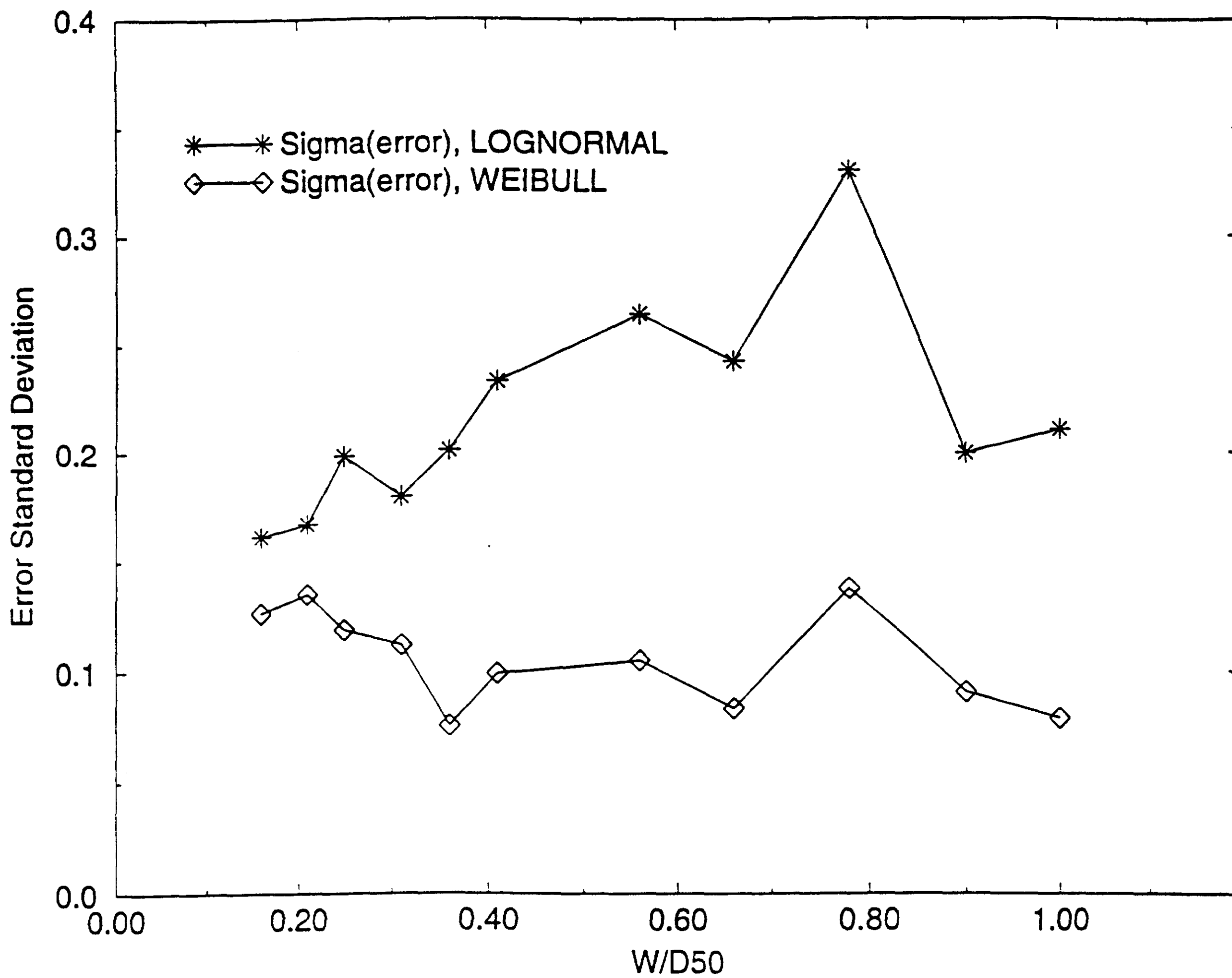

Figure 4.6 Comparison of the error in fitting a lognormal distribution vs a Weibull distribution in the case of bamboo segments. The Weibull distribution fits better the for a wide range of values of W/D_{50} ($0.1 < W/D_{50} < 1.0$).

Chapter 5

Implementation in the Electromigration Simulation Tool

5.1 The Electromigration Simulation Program

The electromigration simulation program [Knowlton, Park and Andleigh, unpublished], allows the determination of the electromigration-induced stress-evolution in interconnect lines. The program uses the finite differences method along with other numerical methods to solve numerically the Korhonen equation A.5, and determine the stress profile along an interconnect line as a function of time. This work improves upon previously existing efforts [20, 33] by allowing for non-zero diffusivity in bamboo regions, allowing for stress dependent diffusivities, and by allowing for interaction between polygranular clusters. The boundary conditions can be taken as either zero stress $\sigma = 0$ which is consistent with a line ending in large contact pads, or zero atomic flux $J = 0$, which is consistent with a line ending at a tungsten stud. Among the features offered by the simulation tool is the possibility of determining the behavior of an interconnect line with a variable width. This feature, of a major practical impact, has yet to be fully explored: the microstructure of large populations of lines with variable widths have to be simulated before final conclusions can be drawn as to the effect of variable width in

conjunction with microstructural characteristics on the reliability of a population of interconnects.

Applying this numerical model to determine the effects of a single polycrystalline cluster as compared to two clusters in an interconnect led [30] to the conclusion that polygranular clusters interact, causing a stress profile highly dependent not only on the cluster lengths, but also on the distance separating clusters. Figure 5.1 and 5.2 show the stress evolution profile in these two cases for short, intermediate and long times. Comparing these figures, it is clear that the maximum stress achieved in the line with two clusters is significantly greater than that achieved in the case of a line with a single cluster of the same total length. The degree of coupling between adjacent clusters depends upon the spacing between the clusters and the diffusivity ratio $D_{cluster}/D_{bamboo}$. Figure 5.3 shows the maximum stress as a function of time for pure Al ($D_{cluster}/D_{bamboo}=10^4$) lines with several cluster spacings. The curves for isolated clusters are also shown as a reference. As cluster spacing decreases, cluster interaction occurs at earlier times. The maximum stress achieved increases when the distance between clusters decreases.

5.2 Reliability of Realistic Lines Generated with the Grain Growth Program

Studying one and two cluster lines helps quantify the degree of stress coupling between clusters, but the overall impact of this phenomenon on the reliability of actual interconnects is unclear since real lines contain many clusters with a variety of lengths

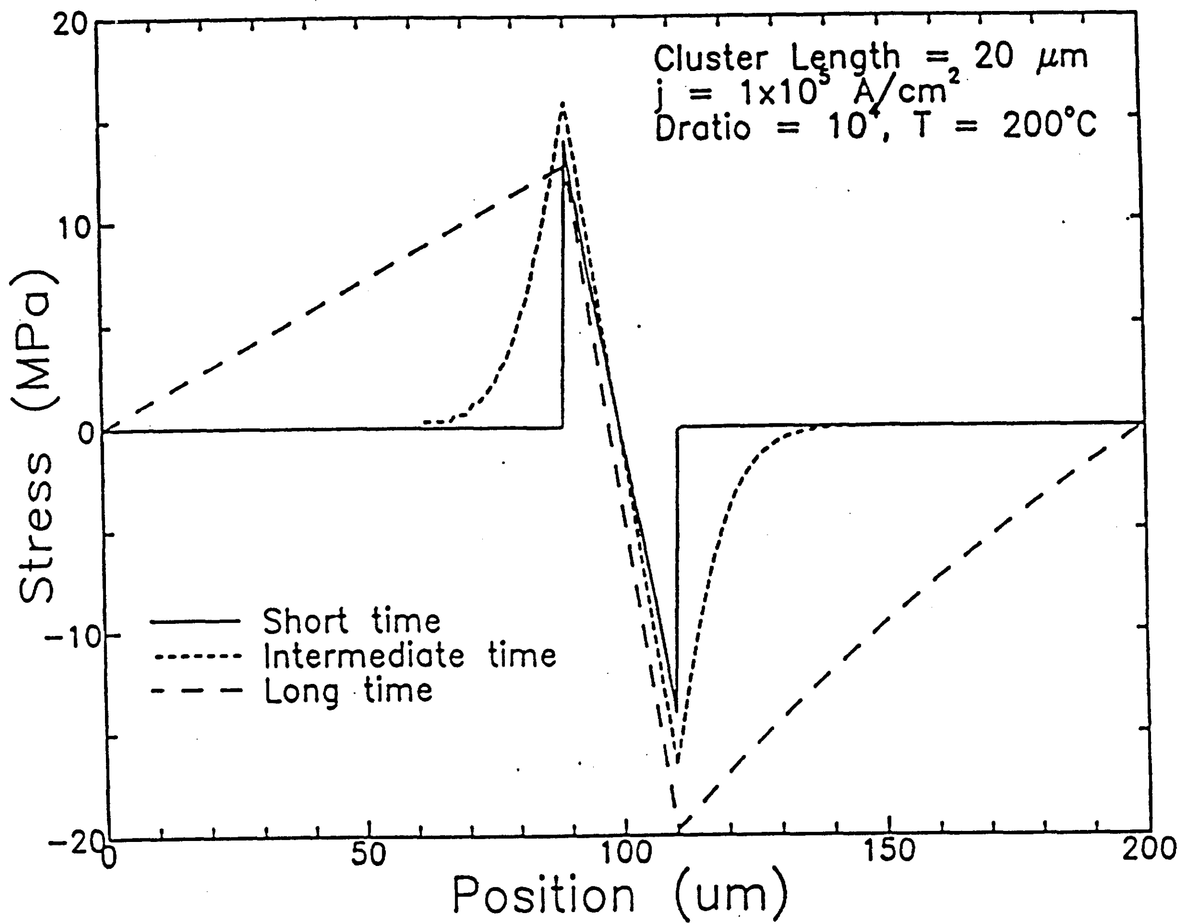

Figure 5.1 The stress as a function of position for a line containing a single 20 μm long polygranular cluster.

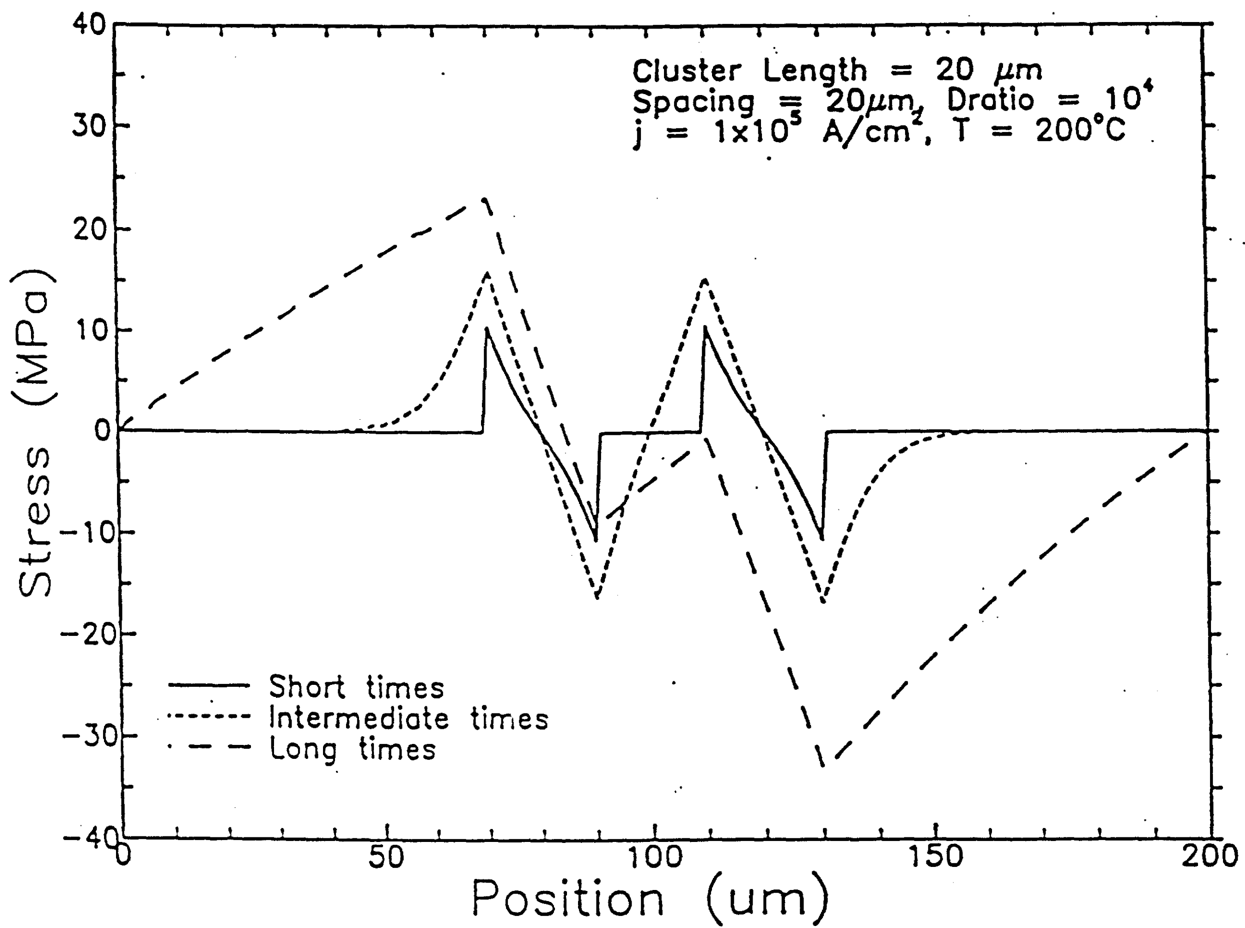

Figure 5.2 The stress as a function of position for a line containing two 20 μm long polygranular clusters separated by 20 μm. The stress profiles from each cluster begin to interact at intermediate times, leading to larger stresses than either cluster could support independently.

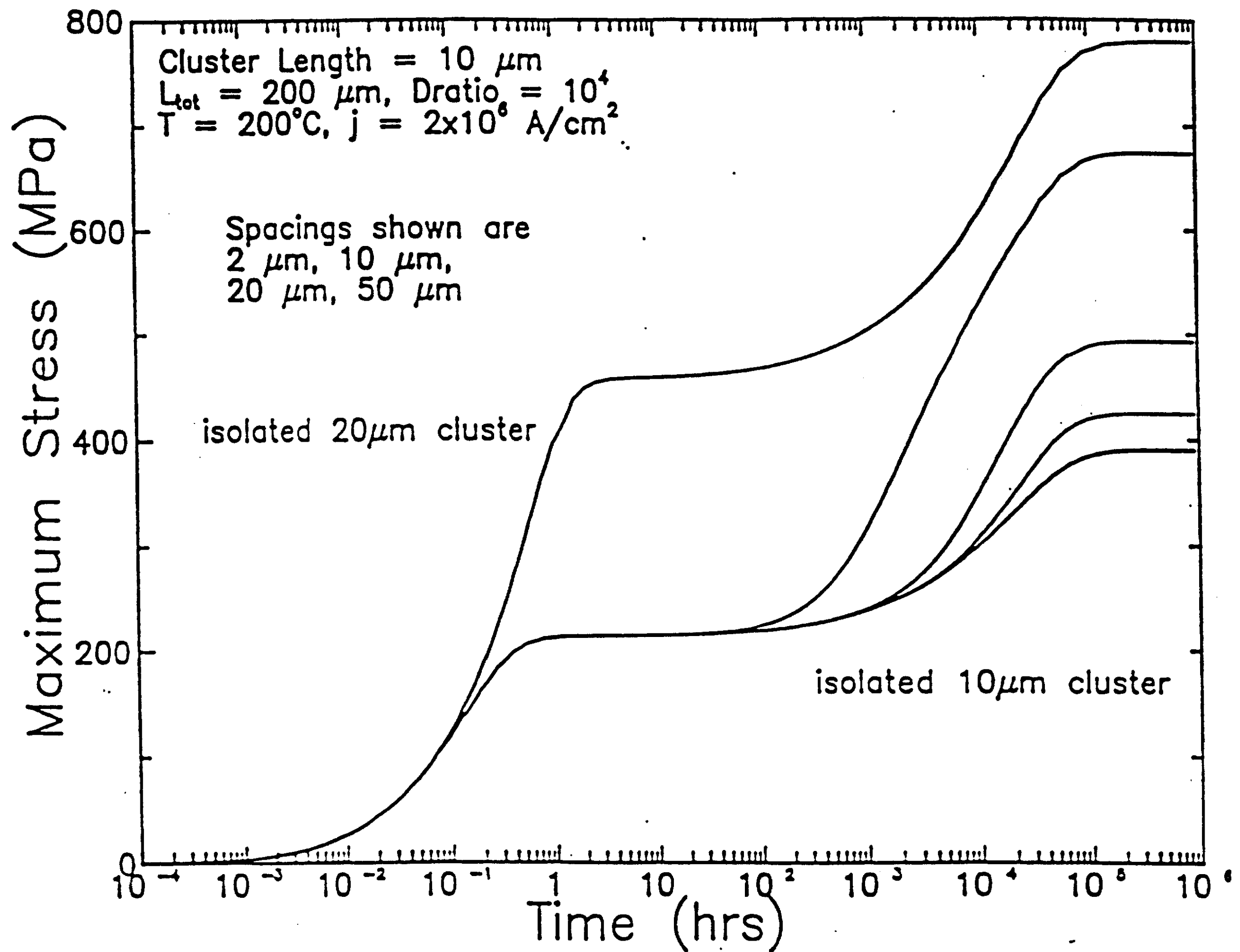

Figure 5.3 The maximum stress as a function of time for pure Al lines with two 10 μm long polygranular clusters with a variety of spacings at a typical test current density. Curves for isolated clusters are also shown as a reference.

and spacings. Exploring the full implications of cluster interactions requires simulation of stress evolution in populations of lines with realistic microstructures. This was achieved [30] by using the electromigration model in conjunction with the grain growth simulator [16-17, 29]. As we have seen, the simulator is capable of generating realistic continuous film microstructures, patterning lines from a continuous film, and modeling grain growth during an anneal. The combination of the Korhonen model with the grain growth simulator yields an extremely powerful and flexible tool for investigating interconnect reliability. Large populations of lines can be generated and tested quickly, allowing statistical differences in both microstructure and failure rate to be characterized.

To analyze the effect of microstructure on the stress evolution in straight lines and on their reliability, the grain growth simulator was used to generate realistic continuous film structures. The etching program was then used, as discussed in previous sections of this thesis, to generate lines of various width and lengths. Once realistic line microstructures were generated, the stress evolution behavior was calculated for a population of similar lines (i.e., lines with the same geometry and process history). The maximum stress as a function of time for a population of ten as-patterned lines with zero stress boundary conditions and $W/D_{50} = 0.5$ are shown in figure 5.4. The variation in grain sizes in the continuous film translates into a variation in the cluster length and bamboo length distributions from line to line, accounting for the observed variation in stress evolution behavior. The information in figure 5.4 can be used to determine failure time distributions, if we consider, as previously suggested, failure of a line to occur when the maximum stress in the line reaches a critical value σ_{cr}. The failure time statistics for a

given population are sensitive to the value of this critical stress. If σ_{cr} is low, all lines quickly fail via polygranular failure mechanisms, and the failure time distribution is monomodal with a small deviation in the times to failure. At high values of σ_{cr}, however, the effect of microstructure is more important as transgranular failure mechanisms dominate, so that the distribution of failure times is monomodal with a high deviation in the time to failure. At intermediate values of the critical stress both failure mechanisms are observed and a bimodal failure time distribution is observed. All three cases are illustrated in figure 5.5, where polygranular failures are marked with stars, and transgranular failures are marked with circles.

5.3 Using the Statistical Model to Predict Reliability of Interconnects

As we have seen in the conclusion of chapter 4, the statistical models developed for the distributions of bamboo lengths and polygranular cluster lengths in interconnect lines can be used to generate realistic lines with realistic microstructures. This information can then be fed to the electromigration simulation program in order to study stress evolutions and failure time statistics without actually having to run the grain growth simulator to generate populations of lines.

We have developed [32] a web-based software package that can be used to evaluate the reliability of interconnect lines with the desired characteristics. The user is asked to enter the information concerning the number of lines

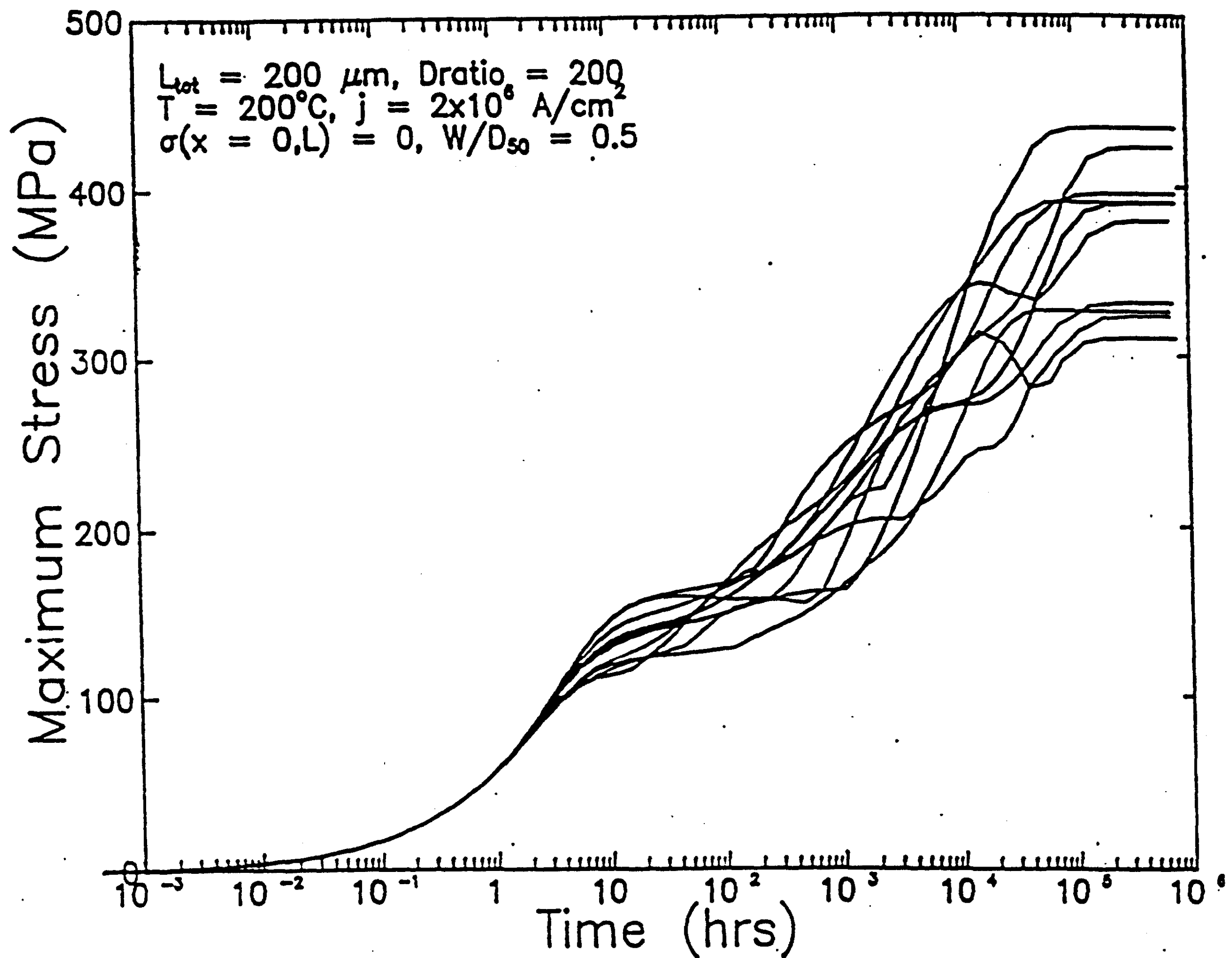

Figure 5.4 The maximum stress as a function of position for 10 as-patterned lines with zero stress boundary conditions. All of these lines have identical process histories. The variation in microstructure from line to line accounts for the variation in stress evolution behavior [30].

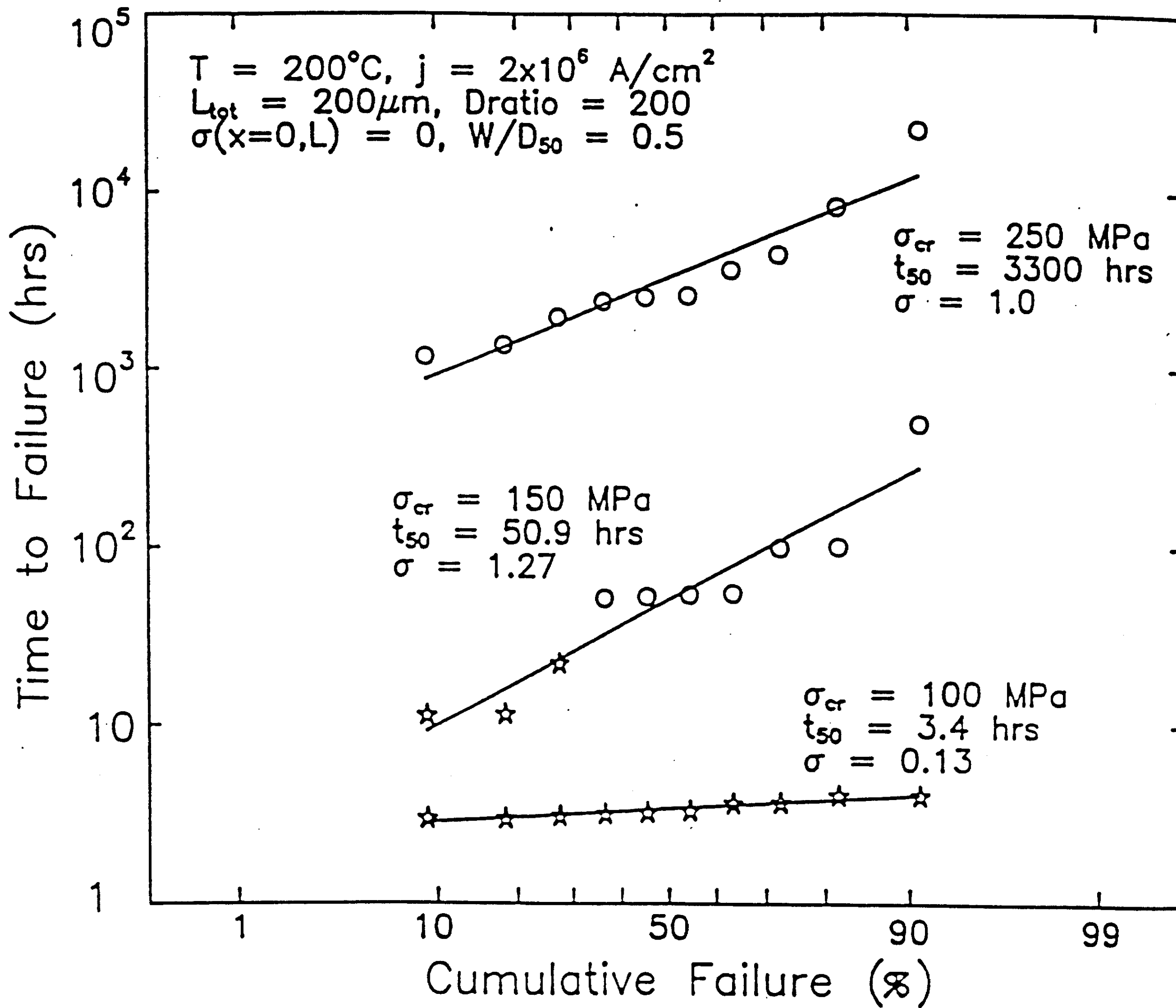

Figure 5.5 Lognormal plot of failure time distributions for the lines considered in figure 5.4 for small, intermediate and large values of σ_{cr}. Polygranular failures are denoted by stars, and transgranular failures are denoted by circles. At intermediate values of σ_{cr}, two failure mechanisms are active, resulting in a bimodal distribution [30].

to simulate, their different geometrical characteristics (width, length), the median grain size, the current density they are subjected to, the temperature, as well as the different physical parameters necessary for the determination of the stress evolution profile. The program first uses the entered geometrical characteristics to determine the statistical microstructure parameters for the bamboo and cluster length distributions. The sub-program *emsim_gen* then generates lines with the corresponding bamboo and cluster length distributions. Finally the program feeds the information into the electromigration simulator, and failure times are determined for the critical stress chosen by the user. The current version of the package is running on the Web and can be viewed at the following address: *http:// nirvana.mit.edu/cgi-bin/emsim/emsim.pl.* The input and output pages are shown in figure 5.6. The failure time statistics predicted using this new tool for lines with the same characteristics as the ones in the previous section are given in figure 5.7. The variations observed in the median times to failure and deviation in the times to failure, in comparison with the results of the earlier calculation (figure 5.5), where the lines were generated with the grain growth simulator, have led us to repeat both simulations for two new populations of ten lines, one set generated with the grain growth simulation (figure 5.8), and the other set with the program *emsim_gen* using a Weibull length distributions (figure 5.9). The variations observed between the two populations generated with the growth program (figures 5.5 and 5.8) are of the same order of magnitude as the variations between populations generated with the growth program and generated directly with Weibull length distribution functions (figures 5.5 and 5.7).

Netscape: EMSIM: Electromigration Simulation

File Edit View Go Bookmarks Options Directory Window Help

Location: http://nirvana.mit.edu/cgi-bin/emsim/emsim.pl

What's New? What's Cool? Destinations Net Search People Software

EMSIM 1.0
Electromigration Simulation

Username: valid Key:

Email address: fayad@mit.edu

Length (microns) = 100 (10 <= L <= 1000)

Width (microns) = 1

D_{50} (microns) = 4

Temperature (°C) = 313

Current Density (A/cm²) = 1.5e6

Submit to EMSIM

Clear Inputs

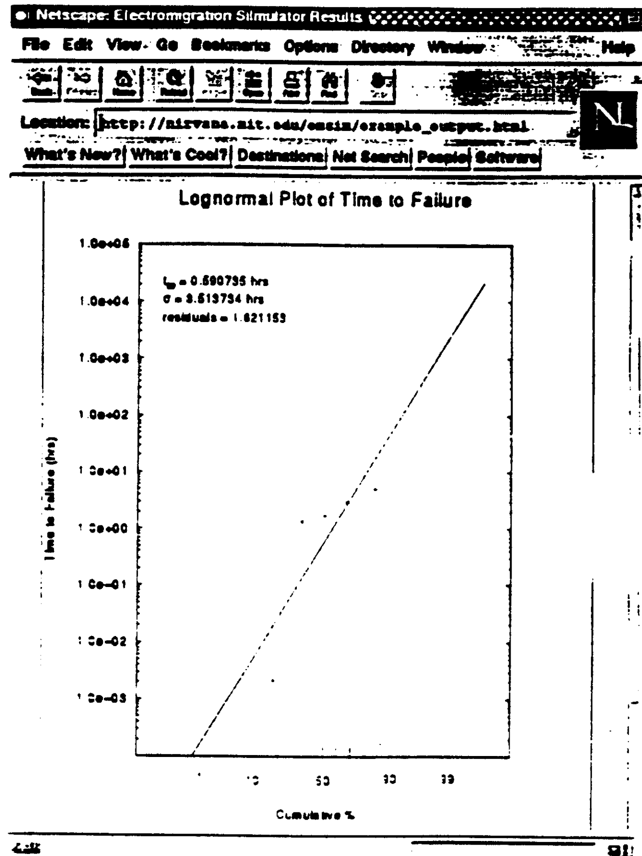

Figure 5.6 The Web interface for the electromigration simulation package. Interconnect lines are generated and electromigration simulations are performed according to the conditions entered by the user. A lognormal plot of the failure times is then displayed to the user.

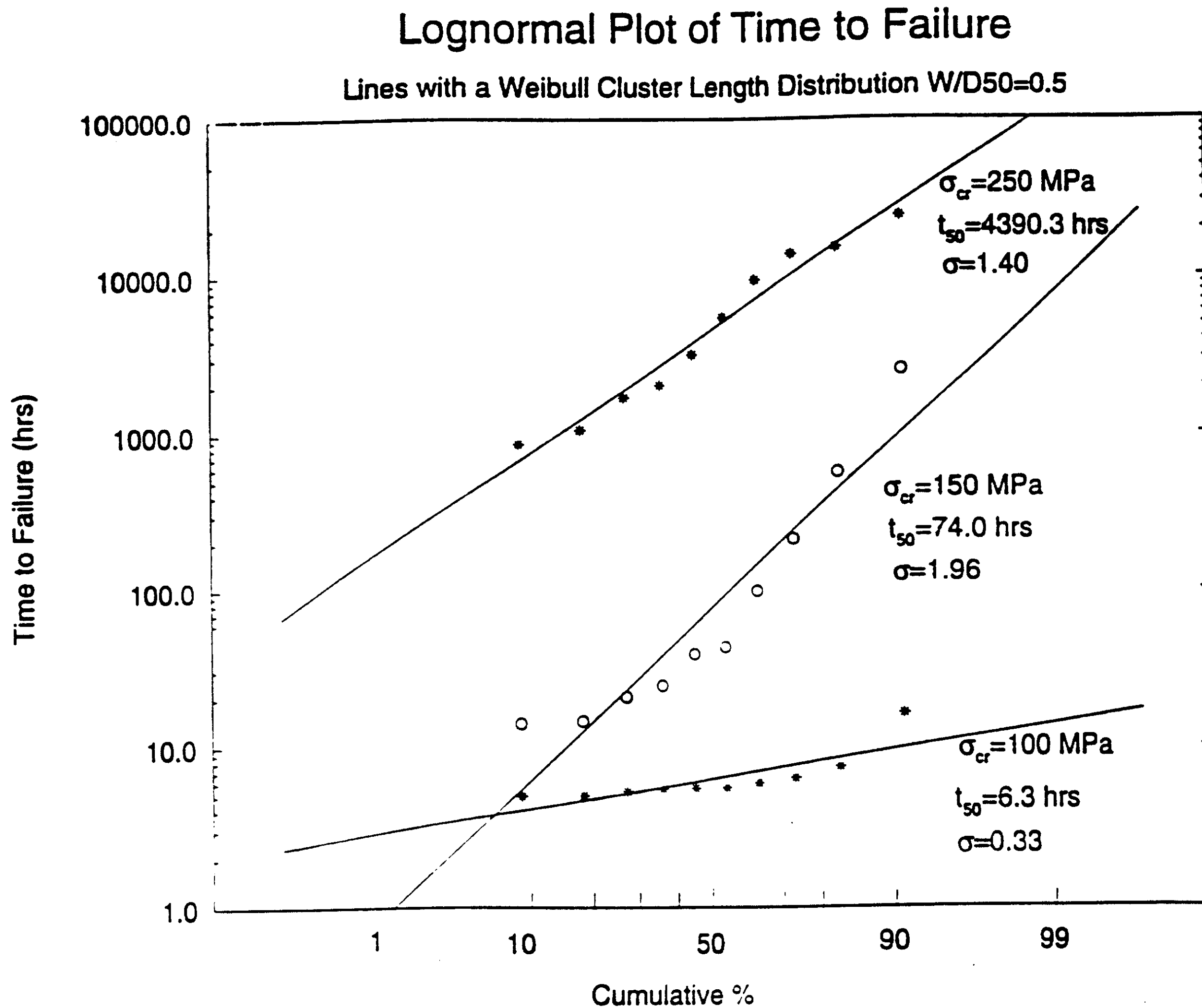

Figure 5.7 Lognormal plot of failure time distributions for 10 lines generated with a Weibull distribution of cluster lengths.

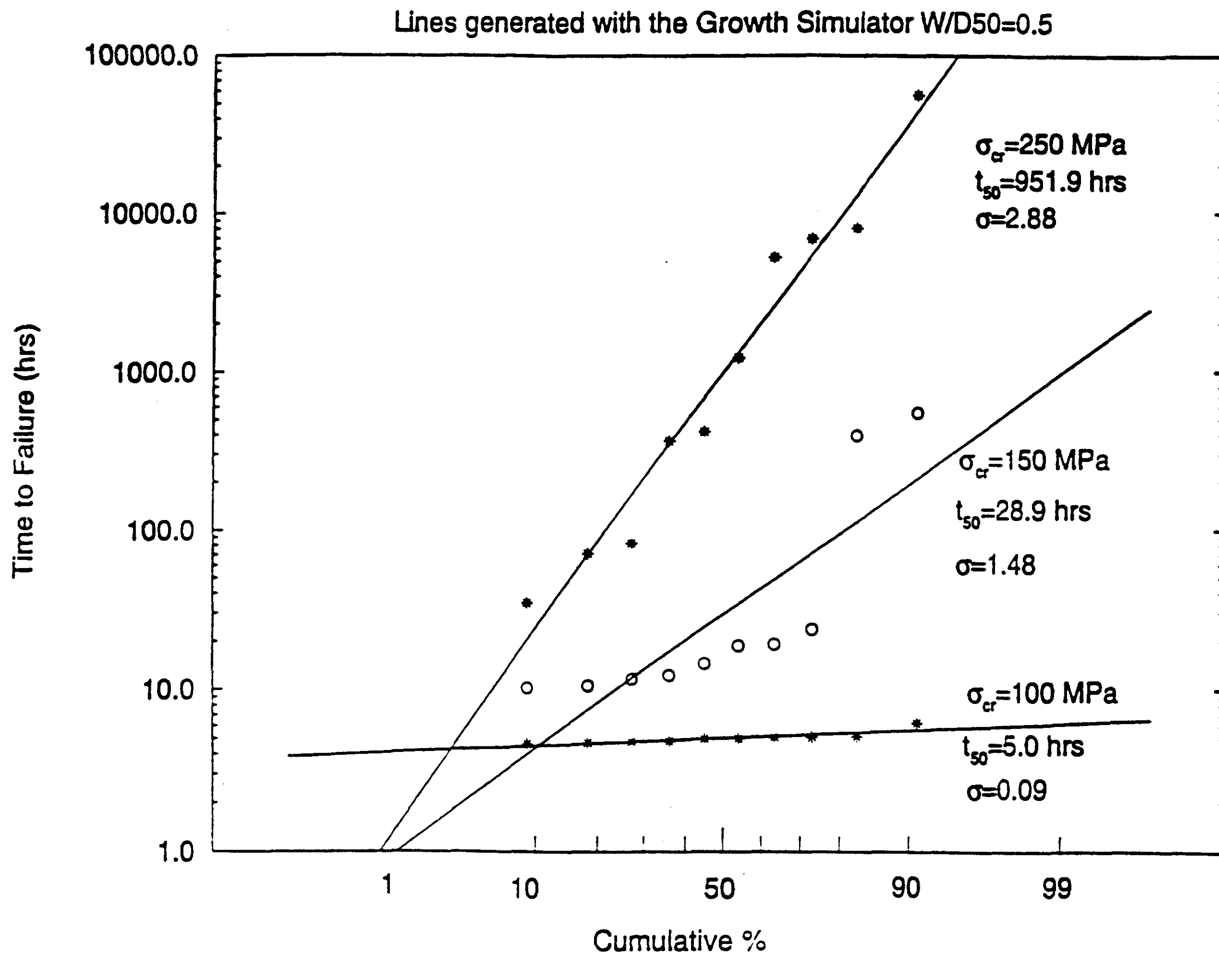

Figure 5.8 Lognormal plot of failure time distributions for 10 lines generated with the grain growth simulator under the same conditions given in figure 5.5.

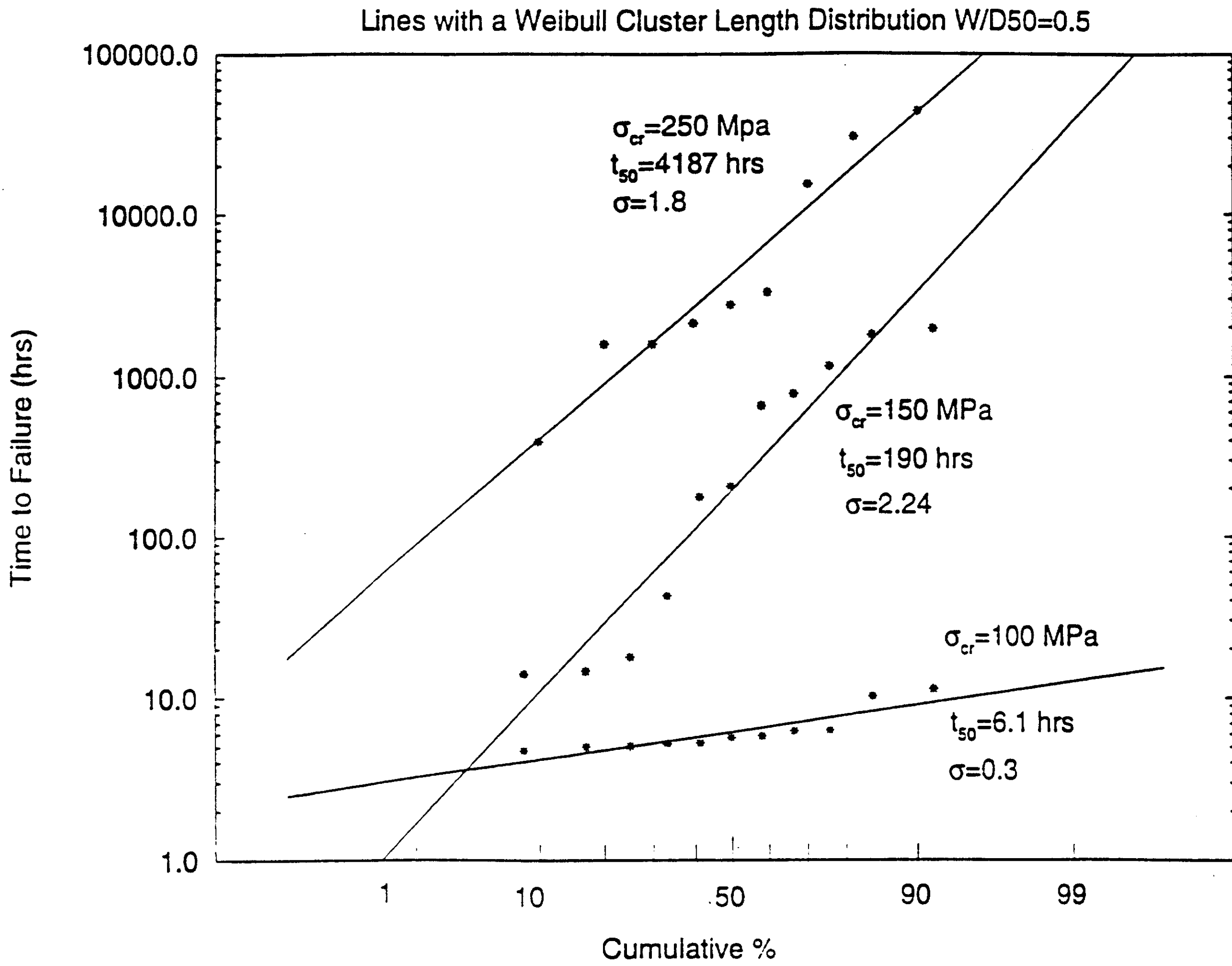

Figure 5.9 Lognormal plot of failure time distributions for 10 lines generated with a Weibull distribution of cluster lengths. This population is different than the one in figure 5.7 but with the same characteristics.

We can extract from these calculations two major conclusions. The first one is that the failure time predictions obtained by using the program generating lines with Weibull length distributions are not inconsistent with the ones obtained by using the grain growth simulator. The second conclusion is that there are a lot of variations in the failure statistics among populations of interconnects formed of only ten lines. Using emsim_gen allows the quick simulation of much larger populations in order to more accurately predict lifetime statistics. Figure 5.10 shows the failure time distribution for a population of fifty lines generated with *emsim_gen*. It is also important to note that with the larger populations represented in figure 5.10, evidence for multiple failure mechanisms is seen for all critical stresses.

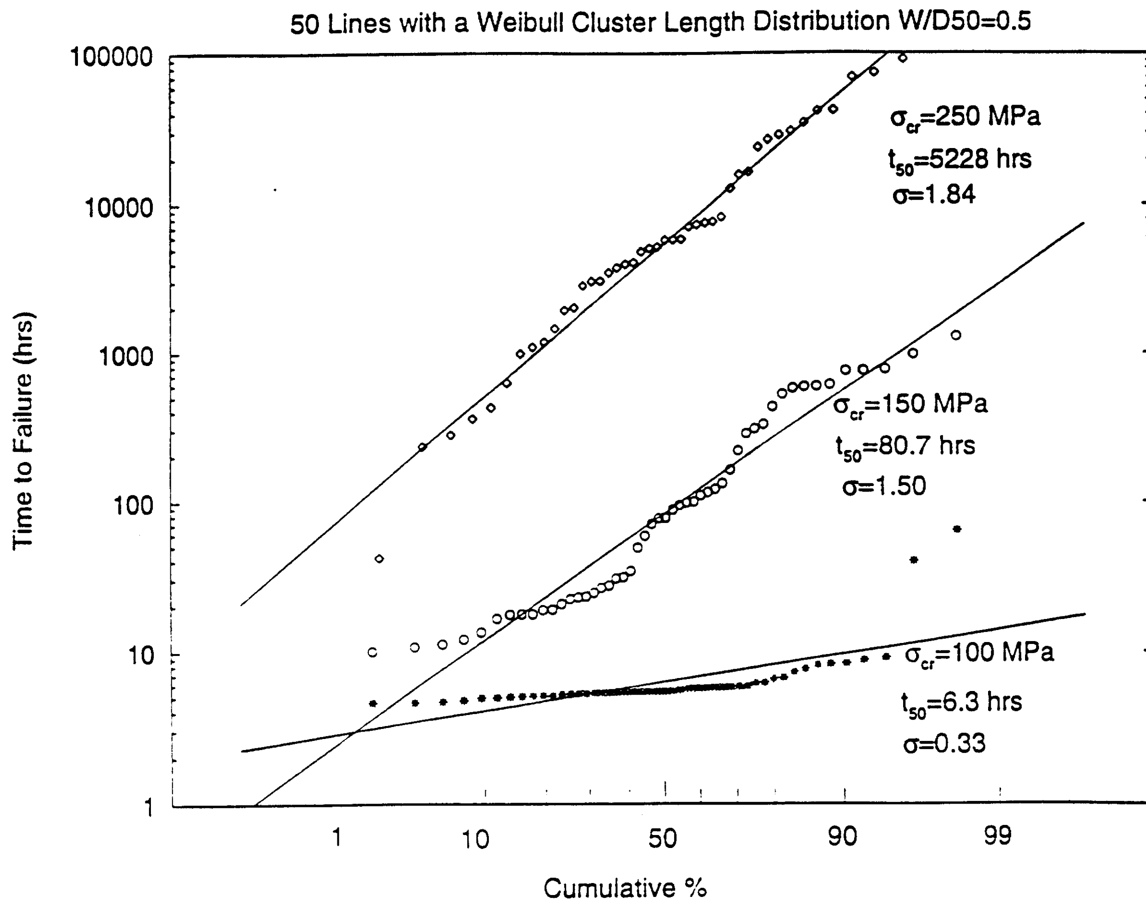

Figure 5.10 Lognormal plot of failure time distributions for a population of fifty lines generated with a Weibull distribution of cluster length.

Chapter 6

Immediate Tasks and Future Perspectives

6.1 Exploring As-Patterned General Features

In an effort to further understand the impact of microstructure on interconnect reliability, the pattern program has been used to investigate microstructural statistics of as-patterned straight line interconnects. We have concluded that the cluster length distribution as well as the bamboo length distribution are well described by Weibull distributions within a wide range for W/D_{50}, but in the case of clusters, we have seen that for relatively wide lines ($W/D_{50}>0.5$) the lognormal distribution provided a better approximation. A unifying description, using the gamma distribution, is currently being explored and expected to provide a better model for both cluster and bamboo length distributions. Exploring as-patterned straight lines has also led us to discover the end effects on cluster length distributions. We have seen that these effects are important only for relatively short lines, when the line length is comparable to the maximum cluster length. We are currently working on developing an analytic model for the impact of end effects on cluster length distribution.

Another potential application of the pattern program is to assess and analytically model the via/cluster interaction. The vias, usually made of Tungsten, form the connections between different layers of metal in a circuit. They constitute sites of current

crowding and therefore potential electromigration induced failure. Depending on the position of the via along the interconnect line, it can either hit a polygranular cluster or a bamboo segment, which is crucial in terms of reliability impact. A correct assessment of the interaction between vias and clusters, as a function of the line characteristic as well as the vias sizes, is therefore important for a better understanding of interconnect reliability.

The pattern program which has so far been used to investigate as-patterned straigth lines has a more general major application, the simulation of interconnects with general geometries, which has yet to be fully explored. Two important common features are, as we have seen, T's and L's. If we take the case of the L structure, the number of geometrical characteristics describing the feature is 4 instead of 2 for the simple rectangular pattern (representing finite straight interconnects). Figure 6.1 shows that this number goes down to 3 in the particular case of constant width. The case of a T is even more complex, and we can already see that the relation between geometry and microstructure is less obvious. Nevertheless, it is very important from a practical point of view, since these types of structures are common, to investigate the possible existence of a simple analytic model capturing the essential part of the relationship between geometrical characteristics and film structure statistical parameters on one side, and microstructural statistical characteristics of such features on the other.

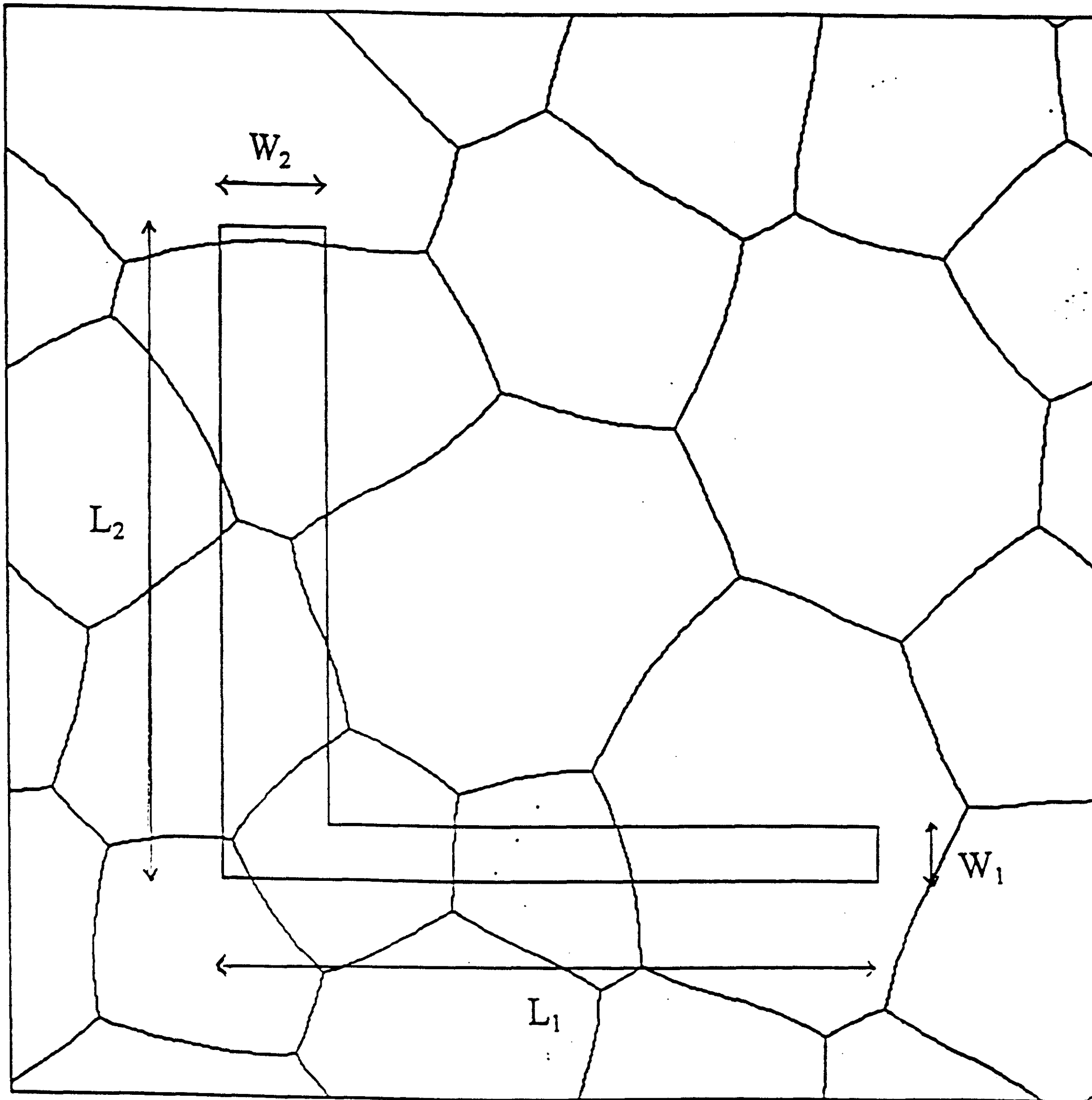

Figure 6.1 4 geometrical parameters for an L structure vs only 2 for a simple rectangular line (the width W and length L).

6.2 Post-Patterning Annealing in General Shapes

Post-patterning annealing causes grain growth in interconnects. This leads to a more reliable structure since the number and length of high diffusivity polygranular clusters decrease, while the length of lower diffusivity bamboo segments increases. In a similar way, pre-patterning annealing of the film the interconnects are etched from gives, for a given set of geometrical parameters (line width, etc.), a structure more evolved toward a fully-bamboo state and, therefore, more reliable. In order to quantify the beneficial effects of pre-patterning or post-patterning annealing-induced grain growth, it is necessary to accurately model microstructure evolution.

After nucleation and growth-to-impingement, a thin film may evolve through 2-D grain growth. Grain growth is a thermally activated process by which the average grain size of a material increases. In the case of thin films, the driving forces for such a phenomenon are, primarily, capillarity (grain boundary energy), surface/substrate interface energies and strain energy density [31]. In the case of idealized, capillarity-driven grain growth, grain boundaries are assumed to move at a velocity, v, proportional to their local curvature κ, according to $v = \mu\kappa$, where μ is a mobility constant [24]. The boundaries are also assumed to meet at triple junctions to form 120° angles, consistent with the assumption that all boundaries have uniform energy. In the simulation, each boundary is, as we have seen, represented by an array of points. Grain growth is simulated by alternately moving the points describing the grain boundaries and

repositioning the grain boundary triple junctions. In simulations of idealized 2-D grain growth, a steady state structure is reached, where any further evolution occurs self-similarly [25], i.e. with a conserved topological structure. In this growth regime, the average grain diameter increases linearly with the square-root of time [25].

However, idealized 2-D grain growth is rarely observed experimentally. Instead, grain growth is found to stagnate when the average grain size approaches 2 or 3 times the thickness of the film [26, 27]. Mullins [28] has proposed that this stagnation is due to grain boundary grooving at the intersections of the grain boundaries with the film surfaces. Under certain conditions, these grooves will trap or pin migrating boundaries. This effect has been included in the existing grain growth simulator by assuming that boundaries with curvature below a certain critical curvature, κ_{crit}, are unable to migrate. This procedure has permitted us to generate fully stagnant structures which closely resemble those observed experimentally. These stagnant grain structures have a lognormal grain size distribution with an average grain size proportional to the inverse of the critical curvature.

Similar considerations of grain boundary energy effects and grain free-surface-energy induced grooving effects, have permitted the modeling of grain growth in etched infinite lines obtained with the *etch* program. In idealized 2-D grain growth grain boundaries meet the side wall of a strip at an angle of 90°. Grooving at the strip side-walls will cause boundaries to meet at angles slightly different from 90°. Modeling the motion of grain boundaries at the strip-walls involves the definition of two critical angles between the grain boundary and the normal to the side-wall [17], the static-groove critical

angle θ_0, which determines if a static grain boundary has enough energy to start moving ($\theta>\theta_0$), and the dynamic-groove critical angle θ_c, which is smaller than θ_0, and which determines if a boundary with steady state motion will continue to move ($\theta>\theta_c$).

The grain boundary motion, handled by the simulation program in the routine *anneal*, only simulates grain growth in semi-infinite line strips with periodic boundary conditions. This is a limiting factor when one needs to assess the effect post-patterning annealing of interconnect elements with arbitrary shapes. One of the main focuses of my future research will be to make the necessary modifications to the existing program, in conjunction with a consistent set of physically coherent assumptions, in order to successfully model grain growth in these cases of great practical importance. A substantial modification concerns the state of an edge triple point approaching a corner of the patterned structure. Such a situation is not encountered in the case of infinite strips with periodic boundary conditions. Modeling this effect will involve the angles of the boundary with both edges defining the corner in question.

Once the simulation of post-patterning annealing is accomplished in these more general cases, the post-patterning annealing interconnect microstructure can be evaluated as a function of the geometrical characteristics as well as the statistical structural parameters of the film. This information can then be used, in conjunction with an appropriate electromigration model, to more accurately assess reliability of real interconnects and of full integrated circuits. Ultimately, these capabilities will enable a *process-sensitive* reliability prediction of an entire circuit *during* the design process. The

resulting concurrent circuit *and* process design will yield a circuit with optimal prformance *and* reliability.

Appendix A

Modeling Electromigration-Induced Stress Evolution in Confined Metal Lines [20]

We consider a thin interconnect line deposited on an oxidized silicon substrate and covered by a rigid dielectric passivation layer, as depicted schematically in figure A.1. The line is considered as embedded in an infinitely thick, rigid dielectric continuum.

We consider the case in which electromigration occurs only through the grain boundaries, neglecting the lattice and interface diffusivity. Grains have a columnar grain structure, so that all grain boundaries are perpendicular to the substrate.

When the line is subjected to a current, the electron-wind constitutes a driving force for atomic diffusion. Since the metal line is constrained by the rigid passivation layer, the electron-wind force will cause resistive stresses to arise along the line. As a result, diffusive fluxes of atoms are quickly affected by differences in the chemical potential (associated with the resistant stress) between different locations of the line as well as by differences in the electric potential (associated with the electron wind). The dominant component of the stress is the hydrostatic one σ, and is related to the chemical potential μ by [ref. 21]:

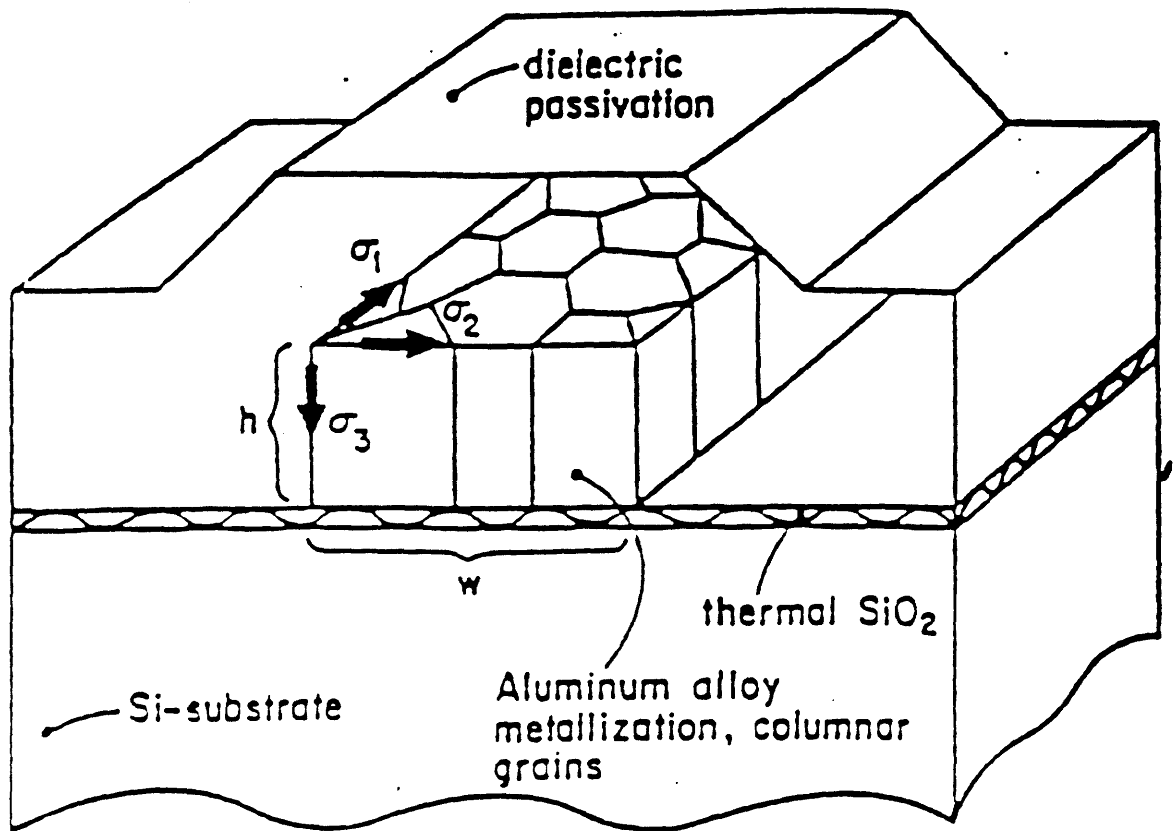

FIG.A·1. Schematic of a confined interconnect line with a columnar grain structure. Also shown are the principal stresses, σ_1 along the line direction, σ_2 in the width (w) direction, and σ_3 in the thickness (h) direction.

$$\mu=\mu_0-\Omega\sigma, \tag{A.1}$$

where Ω is the atomic volume.

The flux of atoms due to a chemical potential gradient $\nabla\mu$ and the electric field E is given by

$$\mathbf{J}=\frac{DC}{kT}(q^*\mathbf{E}+\nabla\mu), \tag{A.2}$$

where C is the concentration of the migrating species, D the effective grain boundary diffusivity and $q^*=Z^*e$ the effective charge. Therefore, for a one-dimensional diffusion flux taken in the positive x-axis direction (also the direction of the electron current):

$$J=-\frac{DC}{kT}(Z^*e\rho j+\Omega\frac{\partial\sigma}{\partial x}), \tag{A.3}$$

where ρ is the resistivity and j the current density.

Assuming that a local equilibrium for vacancies is maintained, the stress increment corresponding to a concentration change can be expressed as

$$-\frac{d\sigma}{B}=\frac{dC}{C} \tag{A.4}$$

where B is an appropriately defined elastic modulus. From the continuity requirement, $\partial C/\partial t=-\partial J/\partial x$, and equations A.3 and A.4, the following evolution equation can be deduced:

$$\frac{\partial\sigma}{\partial t}=\frac{\partial}{\partial x}[\frac{DB\Omega}{kT}(\frac{\partial\sigma}{\partial x}+\frac{Z^*e\rho j}{\Omega})] \tag{A.5}$$

This is the basic 1-D diffusion equation for the stress evolution in interconnects. It can be solved with various boundary conditions. The simplest case is the semi-infinite line

where the flux is blocked at the end, x=0 (J(0,t)=0), for example by means of a tungsten via. The solution can be acquired by Laplace Transformation and is given by

$$\sigma(x,t)=\frac{Z^{*}e\rho j}{\Omega}\left[\sqrt{\frac{4\kappa t}{\pi}}\exp\left(-\frac{x^{2}}{4\kappa t}\right)-x.\,\mathrm{erfc}\left(\frac{x}{\sqrt{4\kappa t}}\right)\right], \qquad (A.6)$$

where κ=DBΩ/kT. Thus, the stress at x=0 becomes

$$\sigma(0,t)=\frac{2Z^{*}e\rho j}{\Omega}\left(\frac{DB\Omega t}{\pi kt}\right)^{1/2}. \qquad (A.7)$$

If failure occurs when the stress at x=0 reaches a critical stress, σ_{cr}, the time to failure is

$$TTF=\frac{kT^{2}}{DB\Omega}\left(\frac{\Omega\sigma_{cr}}{2Z^{*}e\rho j}\right)^{2}=\frac{kT^{2}\Omega}{D_{0}B}\left(\frac{\sigma_{cr}}{2Z^{*}e\rho}\right)^{2}j^{-2}\exp\left(\frac{E_{a}}{kT}\right), \qquad (A.8)$$

where $D=D_0\exp(-E_a/kT)$. This expression takes the form of the empirical equation proposed by Black and predicts the current density exponent of 2.

In the case of the diffusion along a cluster, we are interested in a part of the line of finite length L, where the flux is effectively blocked at both ends. The time dependent solution is expressed in series form, but the steady state solution results in the simple expression:

$$\sigma(x,\infty)=(Z^{*}e\rho jL/\Omega)(1/2-x/L). \qquad (A.9)$$

The maximum steady state stress occurs at both ends, x=0 in tension and x=l in compression, and its magnitude is

$$|\sigma_{max}|=(Z^{*}e\rho jL/2\Omega). \qquad (A.10)$$

This equation gives the same result of the threshold current density relationship originally proposed by Blech and Herring, based on results from drift experiments [22].

This analytical one-dimensional model for describing the stress evolution within a polygranular cluster predicts failure times in a way that matches well the observed behavior. The simplicity of this successful model also allows its application to simulations for statistically significant numbers of appropriately long interconnects, under the wide variety of conditions of importance.

Appendix B

Lognormal and Weibull Distributions

B.1 Lognormal Plot of a Cumulative Distribution Function

Consider a lognormal distribution function of a variable L. The probability density function p.d.f. f(L) is given by:

$$f(L) = \frac{1}{\sigma L\sqrt{2\pi}} \exp[-(\frac{1}{\sqrt{2}\sigma} \ln \frac{L}{L_{50}})^2] \quad \text{(B.1)}$$

Then the variable y=lnL is normally distributed with mean $\ln(L_{50})$ and standard deviation σ,

$$F(y) = \Phi(\frac{y - \ln(L_{50})}{\sigma}), \quad \text{(B.2)}$$

where F(y) is the cumulative distribution function of y, and Φ the standard normal cumulative distribution function. From equation B.2 we directly obtain, by inversion of the Gaussian function,

$$y = \sigma\Phi^{-1}[F(y)] + \ln(L_{50}). \quad \text{(B.3)}$$

This means that if a variable L has a lognormal distribution, then y=ln(L) plots linearly with $x=\Phi^{-1}[F(y)]$, where F is the cumulative distribution function of L and y. Also in this case the slope of the line is the deviation σ and the intercept is $\ln(L_{50})$.

In order to test wether a variable L obeys a lognormal distribution, we can plot its cumulative distribution on lognormal paper, that is we can plot $y_i=\ln(L_i)$ vs $x_i=\Phi^{-1}[F(y_i)]$ for the observed values L_i. The least square method permits the fitting of a linear equation of the type y=a*x+b to the plot that minimizes the error $\sum_i (y_i - ax_i - b)^2$. This yields

$$a = \frac{(\Sigma x_i)(\Sigma y_i) - N\Sigma x_i y_i}{(\Sigma x_i) - N\Sigma x_i^2}, \tag{B.4}$$

$$b = \frac{\Sigma y_i - a\Sigma x_i}{N}. \tag{B.5}$$

where N is the number of observations. a is the least-square estimate of σ and b is the least-square estimate of $\ln(L_{50})$. A measure of the error is given by the standard deviation of the residual $e_i=y_i-ax_i-b$. $\sigma_e(e)=\sqrt{\frac{\Sigma e_i^2}{N}}$, and the accuracy of the linear response is measured with the correlation coefficient $\rho_{xy} = \frac{\mathrm{cov}(x,y)}{\mathrm{var}(x)\,\mathrm{var}(y)}$ that should be 1 for a lognormal distribution.

B.2 Weibull Plot of a Cumulative Distribution Function

For a Weibull Distribution the cumulative distribution function F(L) is given by

$$F(L) = 1 - e^{-(L/\alpha)^{\beta}} \quad \text{(B.6)}$$

where α and β are two statistical parameters. We can notice that this yields

$$L_{50} = \alpha \ln(2)^{1/\beta} \quad \text{(B.7)}$$

In this case the variable y=ln(L) plots linearly with x=ln[-ln(1-F(L))]. As a matter of fact, we will have

$$y = (1/\beta)x + \ln\alpha \quad \text{(B.8)}$$

In order to test wether a variable L obeys a Weibull distribution, we can plot its cumulative distribution on a Weibull paper, that is $y_i = \ln(L_i)$ vs $x_i = \ln[-\ln(1-F(L_i))]$ for the observed values L_i. The least square method permits fitting to a linear equation of the type y=a*x+b to the plot that minimizes the error $\sum_i (y_i - ax_i - b)^2$. This yields the same relations for a and b as in (B.4) and (B.5). a is the least-square estimate of (1/β) and b is the least-square estimate of ln(α). A measure of the error is given by the standard deviation of the residual $e_i = y_i - ax_i - b$. $\sigma_e(e) = \sqrt{\frac{\sum e_i^2}{N}}$, and the accuracy of the linear response is measured with the correlation coefficient $\rho_{xy} = \frac{\text{cov}(x, y)}{\text{var}(x)\,\text{var}(y)}$ that should be 1 for a Weibull distribution.

References

1. H.B. Huntington and A.R. Grone, "Current Induced Marker Motion in Gold Wires", J. Phys. Chem. Solids, **20**, 76 (1961).

2. L. Berenbaum and R. Rosenbergh, "Electromigration Damage of Grain Boundary Triple Points in Al Thin Films", Thin Solid Films, **4**, 187 (1969).

3. E.Kinsbron, "A Model for the Width Dependence of Electromigration Lifetimes in Aluminum Thin-Film Stripes", Appl. Phys. Lett., **36**, 968 (1980).

4. F.M. d'Heurle and P.S. Ho, "Electromigration in Thin Films", in J.M. Poate, K.N. Tu and J.W. Mayer, eds., Thin Films-Interdiffusion and Reactionms, (Wiley, New York, 1978), p. 243.

5. J.R. Black, "Mass Transport of Aluminum by Momentum Exchange with Conducting Electrons", 6th Int. Reliability Phys. Symp., IEEE, p.148, 1967.

6. Y.C. Joo and C.V. Thompson, "Analytic Model for the Grain Structure of Near-Bamboo Interconnects", J. Appl. Phys., **76**, 7339 (1994).

7. Y.-C. Joo, "Electromigration Failure and Reliability of Single-Crystal and Polycrystalline Aluminum Interconnects for Integrated Circuits", Ph.D. Thesis, M.I.T., 1995.

8. J. Cho and C.V. Thompson, "Grain Size Dependence of Electromigration Induced Failures in Narrow Interconnects", Appl. Phys. Lett., **54**, 2577 (1989).

9 H. Kahn, "Electromigration Behavior and Reliability of Aluminum-Based Multilevel Interconnects for Integrated Circuits", Ph.D. Thesis, M.I.T., 1992.

10. K. Wu, W. Baerg, and P. Jupiter, Appl. Phys. Lett. **58,** 1299 (1991).

11. M.M. Tracy, P.W. Davies, E. Fanger, and P. Gartman, in Microstructural Science for Thin Film Metallization in Electronic Applications, ed. by J. Sanchez, S.A. Smith, and N. de Lanerolle, TMS, Phoenix, p. 157 (1988).

12. E. Kinsbron, Appl. Phys. Lett., **36**, 968 (1980).

13 M.A. Korhonen, P. Borgesen, D.D. Brown, and C.-Y. Li, "Microstructure Based Model of Electromigration Damage in Confined Line Metallizations in the Presence of Thermally Induced Stresses", J. Appl. Phs., **74**, 4995 (1993).

14. Y.-C. Joo and C. V. Thompson, MRS Symp. Proc. **338**, 319 (1994).

15. M. J. Attardo, R. Rutledge, and R.C. Jack, J. Appl. Phys. **42**, 4343 (1971).

16 D. T. Walton, H. J. Frost, and C. V. Thompson, MRS Symp. Proc. **225**, 219 (1991).

17. D. T. Walton, M.S. Thesis, Thayer School of Engineering, Dartmouth College, 1991.

18. B. K. Knowlton, J. J. Clement, and R. I. Frank, "Coupled Stress Evolution in Polygranular Clusters and Bamboo Segments in Near-Bamboo Interconnects", MRS Symp Proc. **391**, (1995).

19. D. D. Brown, J. E. Sanchez Jr., P. R. Besser, M. A. Korhonen, and C.-Y. Li, MRS Symp. Proc. **391**, (1995).

20. M. A. Korhonen, P. Borgesen, K. N. Tu, and C.-Y. Li, "Stress Evolution Due to Electromigration in Confined Metal Lines", J. Appl. Phys. **73**, 3790 (1993).

21. C. Herring, J. Appl. Phys. **21**, 437 (1950).

22. I. A. Blech, "Electromigration in Thin Gold Films on Titanium Nitride", J. Appl. Phys. **47**, 1203 (1976).

23. W. A. Johnson and R. F. Mehl, Trans. AIME, **135**, 416 (1939).

24 W. W. Mullins, "Two Dimensional Motion of Idealized Grain Boundaries", J. Appl. Phys., **27**, 900 (1956).

25 H. J. Frost and C. V. Thompson, "Computer Simulation of Microstructural Evolution in Thin Films", J. Electronic Materials, **17**, 447 (1988).

26 P. A. Beck, M. L. Holtzworth, and P. R. Sperry, trans. AIME, **180**, 163 (1949).

27 J. E. Palmer, C. V. Thompson, and H. I. Smith, "Grain Growth and Grain Size Distributions in Thin Germanium Films", J. Appl Phys., **62**, 2492 (1987).

28 W. W. Mullins, "The Effect of Thermal Grooving on Grain Boundary Motion", Acta metall., **6**, 414 (1958).

29 H. J. Frost and C. V. Thompson, "Simulation of Thin Films Grain Structure I: Grain Growth Stagnation", Acta metall., **38**, 1455 (1990).

30 B. D. Knowlton, "The Effect of Grain Structure and Cu Distribution on the Reliability of Near-Bamboo Al-Cu Alloy Interconnects", Ph.D. thesis, MIT (1997).

31 R. Carel, "Grain Growth and Texture Evolution in Thin Films", Ph.D. thesis, MIT (1995).

32 V. Andleigh, M. Verminski, W. Fayad, unpublished research.